The Effect of Bias polarity Dependence on the DC Electrical Characteristics and sensitivity of Silicon Nanowires for biosensing application

By
Rifat Nigar Pinkey
(ID: 2009-1-80-010)
and
Shams Zinat Tasnim
(ID: 2009-1-80-050)

Submitted to the

Department of Electrical and Electronic Engineering
Faculty of Sciences and Engineering
East West University

in partial fulfillment of the requirements for the degree of
Bachelor of Science in Electrical and Electronic Engineering
(B.Sc. in EEE)

Summer, 2013

Approved By

__________________ __________________

Academic Advisor	Department Chairperson
Dr. Mohammad Mojammel AL Hakim	Dr. Mohammad Mojammel AL Hakim

Approval

The Thesis titled 'The Effect of Bias polarity Dependence on the DC Electrical Characteristics and sensitivity of Silicon Nanowires for biosensing application' submitted by Rifat Nigar Pinkey [2009-1-80-010] and Shams Zinat Tasnim [2009-1-80-050] in the semester of summer 2013 is approved as satisfactory in partial fulfillment of the requirements for the degree of Bachelor of Science in Electrical and Electronic Engineering.

Dr. Mohammad Mojammel AL Hakim
Chairperson Department of Electrical and Electronic Engineering
East West University, Dhaka

Declaration

We, hereby certify that our thesis work solely to be our own scholarly work. To the best of our knowledge, it has not been shared from any source without the due acknowledgement and permission. It is being submitted in partial fulfillment of requirements for the degree of Bachelor of Science in Electrical and Electronic Engineering. It has not been submitted before any degree or examination of any other university.

____

Rifat Nigar Pinkey

____

Shams Zinat Tasnim

Summer Semester
August'2013

Abstract

We investigate the effect of bias polarity on the DC electrical characteristics of p-type silicon nanowires and its effect on the gate sensitivity for possible application as biosensors. A 75 nm thick nanowire with doping concentration of 10^{14} cm^{-3} is investigated for different channel lengths. It is found that when drain and gate voltage both are positive nanowires I_D-V_D characteristics typically exhibit non-linear diode like characteristics with no appreciable conduction up to a certain level of drain bias. The gate sensitivity of nanowires at this mode of conduction is estimated and found to be 18.9%/V for a channel length of 1 μm which reduces to a value of 12.5%/V for the channel length of 100 nm. When gate voltage is positive and drain voltage is negative no appreciable conduction is observed and the gate effect is diminished at short channel lengths which implies that at this mode of conduction p-type Si NW might not be suitable for biosensors. When gate voltage is negative and drain voltage is positive nanowires exhibit less non-linearity and with the increase of negative gate voltages perfectly linear characteristics is achieved through the accumulation of holes in the nanowire by the gate effect. The sensitivity of nanowires at this mode of operation is found to be 11.318%/V and 7.549%/V respectively for 1 μm and 100nm channel length for a gate voltage change from -2v to -1.5V with a drain bias set to 8V. These levels of sensitivity agree very well with the reported sensitivity of silicon nanowire biosensors. However, when both gate and drain voltages are negative a drastic change of the nanowire characteristics is observed and the 75nm thick nanowires NWs are behaving perfectly as a transistor. It is observed that in this mode of operation sensitivity is very high compare to the other modes of operation for all channel lengths. For 1μm channel length, sensitivities obtained are 199.866%/V (when ΔV_G =1-1.5), 154.373%/V (when ΔV_G =1.5-2) and 103.604%/V (when ΔV_G =2.5-2). For 100nm channel length, sensitivities obtained are 35.019%/V (when ΔV_G =1-1.5), 42.058%/V (when ΔV_G =1.5-2) and 38.333%/V (when ΔV_G =2.5-2). This result indicates that for p-type Si NW application of negative voltages to both V_G and V_D are the most viable mode for biosensor operation. We also investigated sub-threshold characteristics of nanowires and it is observed that nanowires can be set to exhibit excellent sensitivity with an appropriate V_G range if it can be ensured that NWs fall within the sub-threshold region of operation. Sensitivity values of 285.713%/V and 174.187%/V are achieved respectively for 1 μm and 100 nm channel lengths with positive drain voltage and negative gate voltages and sensitivity values of 307.6 %/V and 285.7 %/V are achieved respectively for 1 μm and 100 nm channel lengths with negative voltages both at drain and gate by ensuring subthreshold regime of operation. This investigation reveals the requirement of appropriate biasing scheme for highly sensitive biosensor operation and is very significant for nanowire based biosensor applications as transistor behavior can be set by choosing appropriate bias conditions which would allow large conductance charge upon attachment of Biomolecules and a highly sensitive biosensor could be realized.

Acknowledgment

At first, we thank our thesis supervisor, Dr. Mohammad Mojammel AL Hakim who is the chairperson of Department of Electrical and Electronics Engineering of East West University. Without his support we would not have been able to complete this work successfully. We also thank our parents, all the teachers and our friends for their support and encouragement. Finally we bow down our head to our almighty Allah who gave us the patience to finish the task successfully

Authorization page

We hereby certify that we are the sole authors of this thesis. We authorize East West University to lend this thesis to other institutions or individuals for the purpose of scholarly research only after one year of the submission.

____

Rifat Nigar Pinkey

____

Shams Zinat Tasnim

We authorize East West University to produce this thesis by photocopy or other means, in total or in part, at the request of other institutions or individuals for the purpose of scholarly research only after one year of the submission.

____

Rifat Nigar Pinkey

____

Shams Zinat Tasnim

Table of Contents

Page number

Abstract 4
Acknowledgement 5
Table of contents..7
List of figures..9
List of tables 10
Chapter-1: Introduction 11
1.1. Motivation and objective...11
1.2. Organization...11
Chapter-2: Background 12
2.1. Silicon nano wire biosensor 12
Chapter-3: Methodology 16
3.1. Device features and simulation models...16
3.2. Simulation profile...20
Chapter-4: Results..21
Chapter-5: Conclusions, Limitations and Scope of future work 36
5.1. Conclusion...36
5.2. Limitations and scope of future work...37
References 38
Appendix 41

LIST OF FIGURES

Page number

Figure 2.1:Measured output characteristics of junction less accumulation mode silicon nanowire transistors..12

Figure 2.2: Schematic diagram of the structure of Si-nanowire biosensor.................................13

Figure 2.3: Measured sub-threshold characteristics of junction less accumulation mode silicon nanowire transistors 14

Figure 2.4: Electron concentration contour plots in an n-type accumulation mode silicon nanowire transistor ……………………………………………………………………………......15

Figure 3.1: Schematic of the simulated p-type silicon nanowire transistor 16

Figure 3.2: Cross-sectional view of p-type nanowire transistor showing the mesh density used in this simulation 20

Fig. 4.1: Simulated output characteristics (I_D vs. V_D) of Si-nanowire with nanowire thickness of 75nm and doping concentration of $10^{14}cm^{-3}$ for channel length of a) 1µm, b) 500nm, c) 250nm, d) 100nm. Different line represents (I_D vs. V_D) curves for different gate voltages, i.e. 0V, 0.5V, 1V, 1.5V, 2V, 2.5V, 3V 21

Fig. 4.2: Critical voltage vs gate voltage curve of Si-nanowire with nanowire thickness of 75nm and doping concentration of $10^{14}cm^{-3}$ for different channel lengths when both V_G and V_D are positive. Different lines represent curves for different channel lengths,1µm, 500nm, 250nm and 100nm...22

Fig. 4.3: Sensitivity vs channel length curve of si-nanowire with nanowire thickness of 75nm and doping concentration of $10^{14}cm^{-3}$ for different channel lengths when both V_G and V_D are positive ....…23

Fig. 4.4: Simulated output characteristics (I_D vs. V_D) of Si-nanowire with nanowire thickness of 75nm and doping concentration of $10^{14}cm^{-3}$ for channel length of a) 1µm, b) 500nm, c) 250nm, d) 100nm. Different line represents (I_D vs. V_D) curves for different gate voltages, i.e. 0V, 0.5V, 1V, 1.5V, 2V, 2.5V, 3V 24

Fig. 4.5: Critical voltage vs. gate voltage curve of Si-nanowire with nanowire thickness of 75nm and doping concentration of $10^{14}cm^{-3}$ for different channel lengths when v_g is positive and v_d is negative. Different lines represent curves for different channel lengths, 1µm, 500nm, 250nm and 100nm ....……25

Fig. 4.6: Sensitivity vs. channel length curve of Si-nanowire with nanowire thickness of 75nm and doping concentration of $10^{14}cm^{-3}$ for different channel lengths when V_G is positive and V_D is negative 26

Fig. 4.7: Simulated output characteristics (I_D vs. V_D) of Si-nanowire with nanowire thickness of 75nm and doping concentration of $10^{14}cm^{-3}$ for channel length of a) 1µm, b) 500nm, c) 250nm, d)

100nm. Different line represents (I_D vs. V_D) curves for different gate voltages, i.e. 0V, -0.5V, -1V, -1.5V, -2V, -2.5V, -3V...27

Fig. 4.8: Critical voltage vs. gate voltage curve of Si-nanowire with nanowire thickness of 75nm and doping concentration of $10^{14}cm^{-3}$ for different channel lengths when V_D is positive and V_G is negative. Different lines represent curves for different channel lengths, 1µm, 500nm, 250nm and 100nm...28

Fig. 4.9: Sensitivity vs. channel length curve of Si-nanowire with nanowire thickness of 75nm and doping concentration of $10^{14}cm^{-3}$ for different channel lengths when V_G is negative and V_D is positive 28

Fig. 4.10: Simulated output characteristics (I_D vs. V_D) of Si-nanowire with nanowire thickness of 75nm and doping concentration of $10^{14}cm^{-3}$ for channel length of a) 1µm, b) 500nm, c) 250nm, d) 100nm. Different line represents (I_D vs. V_D) curves for different gate voltages, i.e. 0V, -0.5V, -1V, -1.5V, -2V, -2.5V, -3V 30

Fig. 4.11: Sensitivity vs. channel length curve of Si-nanowire with nanowire thickness of 75nm and doping concentration of $10^{14}cm^{-3}$ for different channel lengths when both V_G and V_D are negative 31

Fig. 4.12: Transfer characteristics (I_D vs. V_G) of Si-nanowire with nanowire thickness of 75nm and doping concentration of $10^{14}cm^{-3}$ for channel length of a) 1µm, b) 500nm, c) 250nm, d) 100nm. Different line represents (I_D vs. V_G) curves for different drain voltages, i.e. 0.5V, 1V, 1.5V, 2V where V_G swapped from 5 to -5...32

Fig. 4.13: Sensitivity vs. channel length curve of Si-nanowire with nanowire thickness of 75nm and doping concentration of $10^{14}cm^{-3}$ for different channel lengths for i_d-v_g curve, when V_D is positive 33

Fig. 4.14: Transfer characteristics (I_D vs. V_G) of Si-nanowire with nanowire thickness of 75nm and doping concentration of $10^{14}cm^{-3}$ for channel length of a) 1µm, b) 500nm, c) 250nm, d) 100nm. Different line represents (I_D vs. V_G) curves for different drain voltages, i.e.-0.5V, -1V, -1.5V,- 2V where V_G swapped from 5 to -5...34

Fig. 4.15: Sensitivity vs. channel length curve of Si-nanowire with nanowire thickness of 75nm and doping concentration of $10^{14}cm^{-3}$ for different channel lengths for I_D-V_G curve, when V_D is positive 35

LIST OF TABLES

Page number

Table 3.1: Parameters for Equations 3.1 to 3.7…………………………………………………..18

Table 3.2: Default parameters for equations 3.8 to 3.10 19

Table 3.3: Default parameters of Slotbooms Bandgap narrowing model for equation 3.11.........19

Table A.1: Data table of critical drain voltages at which conduction level of current is $1e^{-4}$, drive currents for ID-VD_VG(pos)_VD(pos) 41

Table A .2: Data table of critical drain voltages at which conduction level of current is $1e^{-12}$, drive currents for ID-VD_VG(pos)_VD(neg)…………………………… 43

Table A.3: Data table of critical drain voltages at which conduction level of current is $1e^{-4}$, drive currents for ID-VD_VG(neg)_VD(pos) 45

Table A.4: Data table of Drive currents for ID-VD_VG (neg)_VD(neg)………………………... 47

Table A.5: Data table of Sub threshold slope(mv/dec), DIBL of different drain voltage for ID-VG_VD(pos)_VG -5 to 5…………………………………………………………………….49

Table A.6: Data table of sub threshold slope(mv/dec), DIBL of different drain voltage for ID-VG_VD(neg)_VG -5 to 5 50

CHAPTER 1: INTRODUCTION

1.1 Motivation and Objective

Over the past decades, semiconductor nanowires have been focused as important research area due to their unique electrical characteristics for biochemical sensors. The reason of interest is due to semiconducting silicon nanowire field effect transistors (Si NW-FETs) have significant influence on disease diagnosis as Si NW-FETs have been shown to function as transducers for level free high sensitivity and direct electrical detection of biomolecules without expensive optical components[1-13]. This ultra-high sensitivity detection can be attributed to their smaller size and large surface to volume ratio, enabling local charge transfers to result in a current change due to a field effect, such as when analytical molecules bind to a specific recognition molecule at the surface of the nanowire [14]. This effect is strong that signal charge at the surface of the nanowires can be sensed because the depletion of accumulation of charge carriers affects the entire cross sectional conductor path of these nanostructures [15].

So far in the literature the sensitivity of Si nanowire biosensors are mainly adjusted by controlling doping, nanowire thickness and clever biochemistry ensuring the targeted proteins to be inside the electrical double layer through the adjustment of solution PH level. It is generally accepted that low doped nanowires with highly constricted dimension would realize highly sensitive biosensors. Quite a variation of the reported sensitivity can also be found in the literature with a detection limit varying from 10fM to 30nM concentrations [8-12, 16-18]. This variation of sensitivity was attributed to the nanowire doping, dimensions and associated chemistry although nanowires inherent DC characteristics is found to be quite variable which might have significant effect on sensitivity. So far there have been no works reported in the literature trying to explain this variation of DC electrical characteristics of SiNWs and its effect on the sensitivity. In this work we first time investigate the bias polarity dependence on the silicon nanowire electrical characteristics. It is found that by choosing appropriate bias silicon nanowires can be set to show linear, non-linear or transistor like characteristics thereby affecting the sensitivity. This result is very significant for nanowire based biosensor applications as transistor behavior can be set by choosing appropriate bias conditions which would allow large conductance charge upon attachment of Biomolecules and a highly sensitive biosensor could be realized.

1.2 Organization

Chapter 2 provides the necessary background work on the electrical Characteristics of silicon nanowires. A number of research papers on Si-NW biosensor have also been surveyed to gain an understanding on the importance of this work.

Chapter 3 describes device structures, simulation methodology and the required models for the simulation.

Chapter 4 describes the simulated results for nanowire thicknesses from 75 nm and for doping densities 10^{14}cm-^{3} for different channel lengths and different bias conditions. The channel length simulated are 1µm, 500nm, 250nm, 100nm.

Finally, in chapter 5, the contribution of this work is summarized and possible areas of future investigations are discussed.

CHAPTER 2: BACKROUND

This Chapter summarizes the background work on the electrical characteristics silicon nanowire, its application as biosensor and relevant theory associated with this work. The conductance changes of silicon nanowires upon attachment of biomolecule have been employed extensively for bio sensing applications. Quite a number of works [19-22] can be found in the literature exploiting this behavior for biosensors. However inherent nanowires electrical characteristics are found to be quite variable although they have been successfully applied for bio sensing application. These are discussed below.

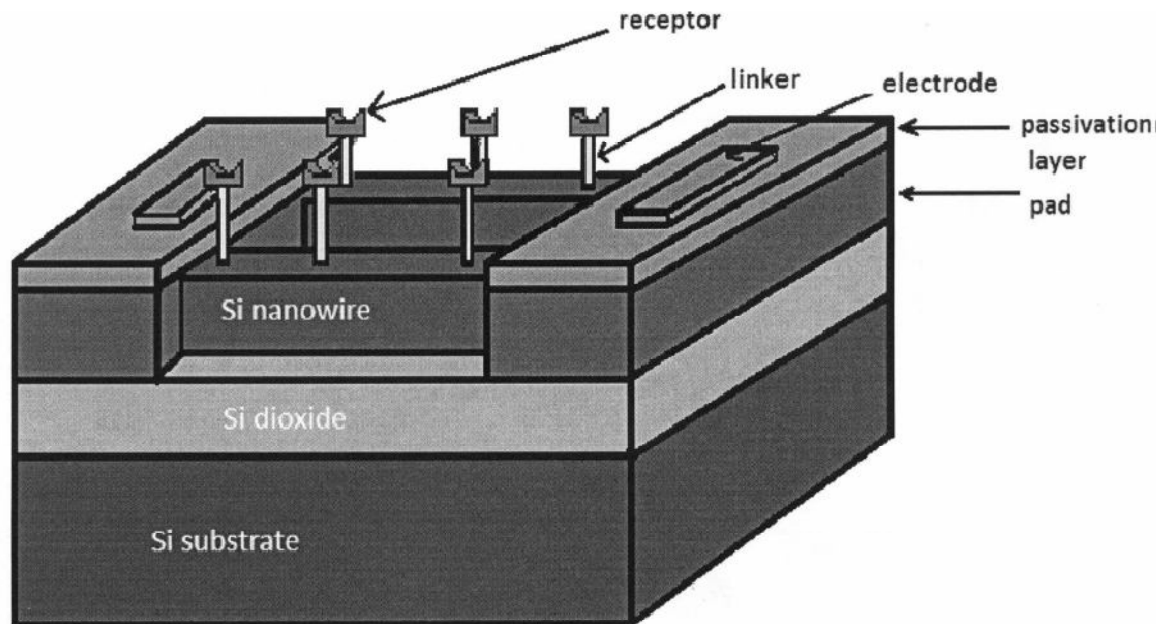

Figure 2.1: Schematic diagram of the structure of Si-nanowire biosensor

A typical nanowire biosensor can be a single or an array of nanowires which is laid on an insulator between source and drain [Figure. 2.1]. Electrodes of these source and drain are isolated by a protection layer. On Si-nanowire surface, target receptors which have the capability of immobilizing the targets, e.g. ions, DNA, proteins are attached by molecular linkers. Due to large surface to volume ratio, the charges associated with the attached molecules can deplete or accumulate entire cross sectional pathway. And hence nanowire conductance gets easily changed. This phenomenon resulted in the most promising breakthrough in the 21st century by possible application of simple nanowire device for disease diagnosis [8-12, 16-18].

Lieber et al. [19] successfully fabricated silicon nanowire biosensors on p-type semiconductor where the typical DC current voltage (I-V) characteristics were linear. The ability of the fabricated biosensors were tested through pH response with or without modifying nanowire surface containing both amino or silanol receptor. It was shown that increase of the solution pH level resulted in the increase of nanowire conductance due to the reduction of the protons in the solution and vice versa

with typical sensitivity around 10% to 20% only. Real time detection of clinically relevant protein streptavidin was also demonstrated down to concentrations of 10pM. Single standard DNA and wild type virus the DF508 also detected. This electrical detection was done to concentration of 60fM. These results exhibited the promise of silicon nanowires as biosensors where nanowire's inherent DC characteristics were linear demonstrated general concept of nanowires just as simple constricted dimension resistors.

Chen et al. [20] fabricated p-type silicon nanowires using a new size reduction method where silicon nanowires have height of 140nm, width of 100nm with triangular structure and a uniform doping concentration of $N_a= 10^{17}$ cm^{-3}. Measured current voltage (I-V) characteristics exhibited typically non-linear diode like characteristics. According to provided I-V curves there were no conduction up to a drain bias of $V_{ds}<1V$. The conduction of nanowires were improved through the application of negative back gate bias thereby increasing the accumulation of holes and at V_{bg} = -20V the I-V characteristics showed linear behaviour. It was noticeable that at small negative V_{bg} I-V characteristics were typically nonlinear. This was attributed to the fixed electronic charge located in the front oxide near the top silicon device layer surface and buried oxide near the bottom of silicon device layer due to reactive thermal oxidation of silicon surface. These nanowires were also successfully sensed pH level of the solution with sensitivity around 40mV/pH.

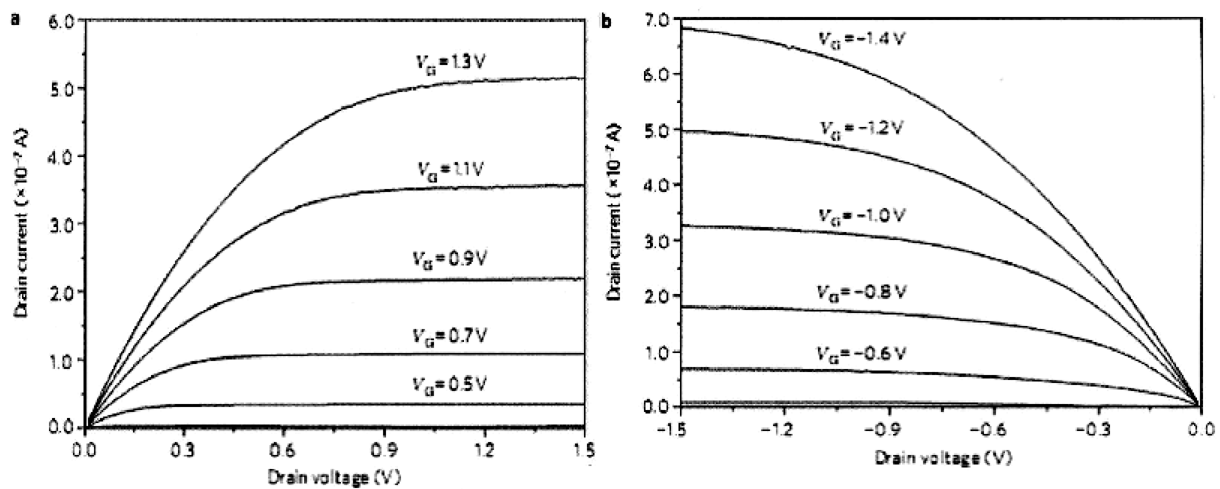

Figure 2.2: Measured output characteristics of junction less accumulation mode silicon nanowire transistors; a) drain current versus drain voltages for an n-type silicon nanowire and b) drain current versus drain voltage for different values for gate voltages for an p-type silicon nanowires. The width, W is 20nm and the gate length, L, is 1µm, such that W/L= 0.02 (courtesy Jean-Pierre Colinge et al. [21].

Most recently, Jean-Pierre Colinge et al.[21] first time reported that Si-Nanowires with a few tens of nanometers wide, thickness of 20nm and uniform doping concentrations around 10^{19} cm^{-3}, behave as transistor than simple resistor. Both p-type and n-type silicon nanowires were fabricated and measured Characteristics showed that both n-type and p-type devices exhibited transistor action. These devices showed near ideal sub-threshold slope of 64mv dec^{-1} and quite decent output

characteristics. Figure 2.2 and 2.3 show the measured sub-threshold and output characteristics of such accumulation mode silicon nanowire transistors.

To explain the behavior of these devices, a simulation was done [24]. Fig. 2.4 shows the operation principle of n-type accumulation mode silicon nanowire transistor. In the sub-threshold region [Fig.2.4(a)], a highly doped channel is fully depleted. At threshold voltage [Fig.2.4(b)], current starts to flow through the center of the channel. Above threshold [Fig.2.4(c)], the channel neutral n- type silicon expands in width and thickness. Further increasing the gate voltage, a completely neutral channel is created [Fig.2.4(d)] when the gate voltage forces saturation of the drain current.

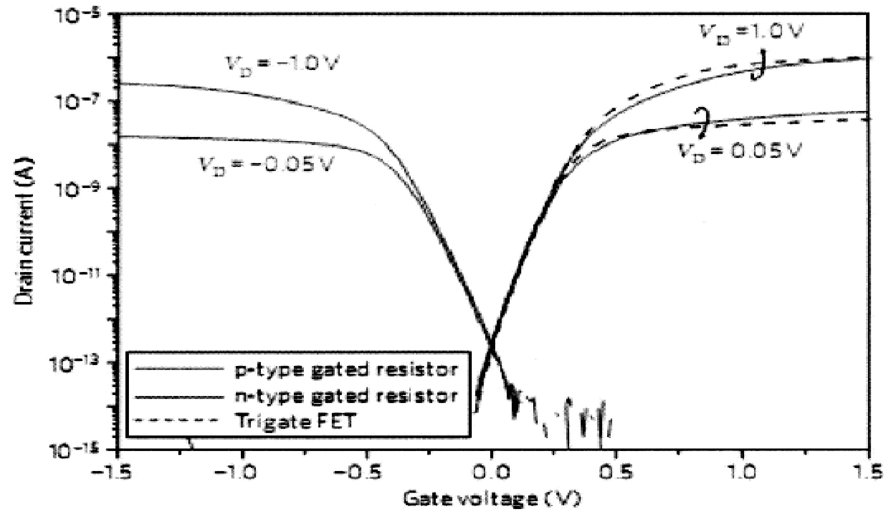

Figure 2.3: Measured sub-threshold characteristics of junction less accumulation mode silicon nanowire transistors. Drain current versus gate voltage for drainvoltagesof±50m V and± 1 V for n-type and p-type silicon nanowires. The width of the nanowires is 30 nm and the gate length, L, is 1 µm (courtesy: Jean-Pierre Colinge et al. [21])

While quite a variable DC I-V characteristics have been obtained after nanowire fabrication and these devices have been successfully employed for bio sensing applications with an excellent detection limit of 10fM, the sensitivity was not promising in most of the reports with values around 10 to 20% only. While these sensitivity variation was attributed to the thickness, doping and associated biochemistry the inherent electrical characteristics might also have an effect on the nanowire sensitivity. To the best of our knowledge there have been no systematic study reported in the literature trying to explain the reason of this variation of DC electrical characteristics of silicon nanowires and its effect on sensitivity. In the literature non-linear I-V characteristics was explained both by Shottky contacts [20] and in case where the contacts were ohmic this was attributed to the surface states associated depletion on inversion of nanowires [22].

In this work we first time investigate bias polarity dependence of silicon nanowire characteristics and shows that drain or gate voltage polarity has significant effect on the DC electrical

characteristics of silicon nanowires. Depending on drain or gate type bias polarity p-type silicon nanowire characteristics found to vary from linear, non-linear diode and transistor like characteristics even though in all cases contacts were ohmic and there were no surface states. This result is very significant for nanowire based biosensor applications as transistor behavior can be set by choosing appropriate bias conditions which would allow large conductance charge upon attachment of Biomolecules and a highly sensitive biosensor could be realized.

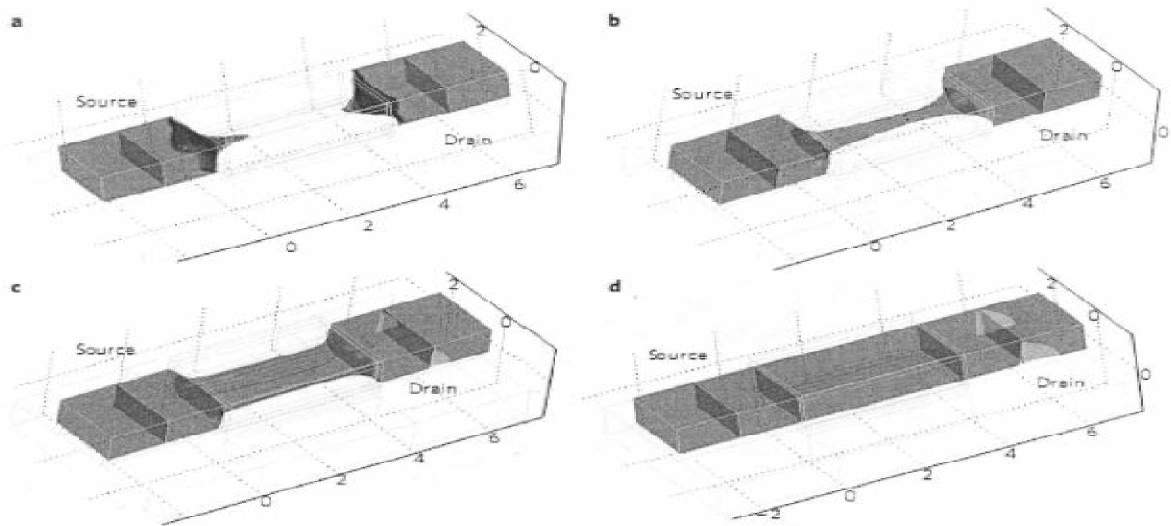

Figure 2.4: Electron concentration contour plots in an n-type accumulation mode silicon nanowire transistor. Plots are taken from simulations carried out for a drain voltage of 50 m V and for different gate voltages: below threshold (V_G<VTH) the channel region is depleted of electrons (a); at threshold (V_G = V TH) a string-shaped channel of neutral n-type silicon connects source and drain (b); above threshold (V_G> V TH) the channel neutral n-type silicon expands in width and thickness (c); when a flat energy bands situation is reached (V_G = VFS »VTH) the channel region has become a simple resistor (d). The plots were generated by solving the Poisson equation and the drift diffusion and continuity equations self-consistently. The device has a channel width, height and length of 20, 10 and 40 nm, respectively. The n-type doping concentration is 1 x 10^{19} cm^{-3}(courtesy: Jean-Pierre Colinge et al. [21])

CHAPTER 3: METHODOLOGY

3.1 Device features and simulation models

The investigation of effect of bias polarity dependence on the electrical characteristics of silicon nanowires were done with the help of numerical simulations using the SILVACO Atlas device simulator [23], installed on a VLSI lab of East West University. A p-type silicon nanowire transistor with 75nm thickness was created on 500 nm oxide substrate (Fig. 3.1) and was simulated for different channel lengths. The gate oxide thickness was 2 nm and the heavily doped poly-silicon layer was used as gate material. In the silicon nanowire, two heavily doped regions on the two sides of the channel were employed to ensure ohmic contacts on the source/drain regions. The gate doping was $10^{21}/cm^3$ and the source/drain regions were also heavily doped with doping density of 1×10^{21} $/cm^3$. The channel doping was 10^{14} cm^{-3}. Here, the gate doping was n-type, whereas the source, the drain and the channel doping was p-type. To contact source to drain and gate, aluminum electrode of 50nm width was chosen.

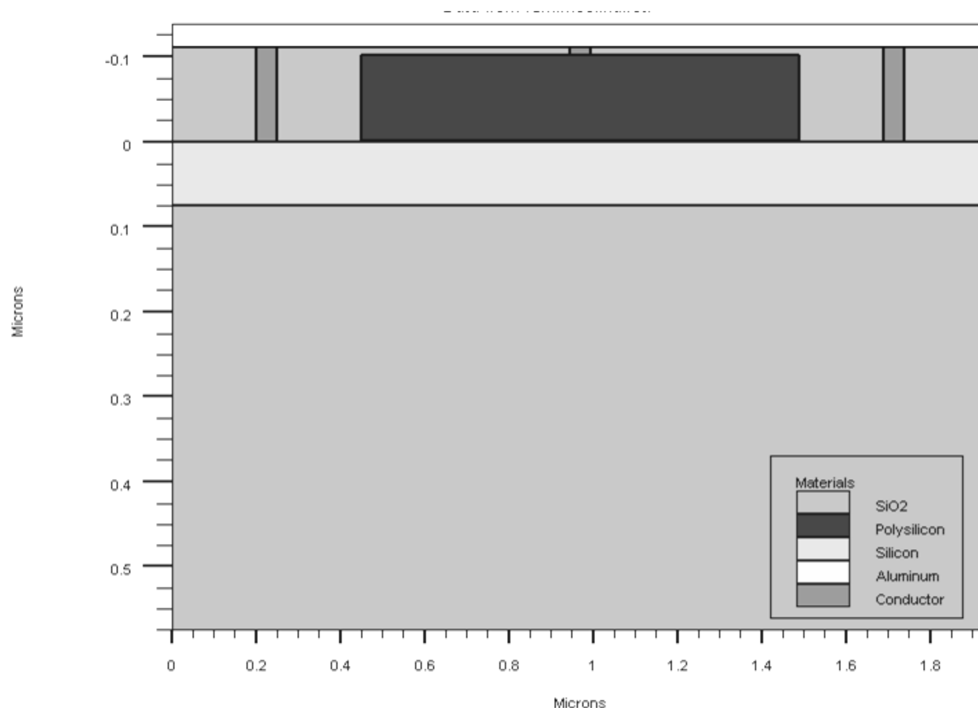

Figure 3.1: Schematic of the simulated p-type silicon nanowire.

Lombardi (CVT) model was used to take account temperature (T_L), perpendicular electric field ($E\perp$), parallel electric field (E//) and doping concentration (N) effects [23]. This model surpasses any other mobility models. In the CVT model, the transverse field, doping dependent and temperature dependent parts of the mobility are given by three components that are combined using Mathiessen's rule. These components are surface mobility limited by scattering with acoustic phonons (μ_{AC}), the mobility limited by surface roughness (μ_{sr}) and the mobility limited

by scattering with optical intervalley phonons (μ_b) are combined using Mathiessen's rule as follows [23]:

μT-1 = μAC-1+ μh-1+ μsr-1 (3.1)

The first component, surface mobility limited by scattering with acoustic phonons equations [23]:

$$\mu_{AC.n} = \frac{BN.CVT}{E_{\perp}} + \frac{CN.CVT\ N^{\tau.CVT}}{T_L\ E_{\perp}^{\frac{1}{3}}} \tag{3.2}$$

$$\mu_{AC.p} = \frac{BP.CVT}{E_{\perp}} + \frac{CP.CVT\ N^{\tau P.CVT}}{T_L\ E_{\perp}^{\frac{1}{3}}} \tag{3.3}$$

The equation parameters BN.CVT, BP.CVT, CN.CVT, CP.CVT, TAUN.CVT, and TAUP.CVT used for this simulation are shown in Table 3-1 [24].

The second component, surface roughness factor is given by [23]:

$$\mu_{sr} = \frac{DELN.CVT}{E_{\perp}^{2}} \tag{3.4}$$

$$\mu_{sr} = \frac{DELP.CVT}{E_{\perp}^{2}} \tag{3.5}$$

The equation parameters DELN.CVT and DELP.CVT used for this simulation are shown in Table 3.1[23].

The third mobility component, mobility limited by scattering with optical intervalley phonons is given by[23]:

$$\mu_{b.n} = MU0N.CVTexp\left(\frac{-PCN.CVT}{N}\right) + \frac{\left[MUMAXN.CVT\left(\frac{T_L}{300}\right)^{-GAMN.CVT} - MU0N.CVT\right]}{1+\left(\frac{N}{CRN.CVT}\right)^{ALPHN.CVT}} - \frac{MU1N.CVT}{1+\left(\frac{CSN.CVT}{N}\right)^{BETAN.CVT}} \tag{3.6}$$

$$\mu_{b.p} = MU0P.CVTexp\left(\frac{-PCN.CVT}{N}\right) + \frac{\left[MUMAXP.CVT\left(\frac{T_L}{300}\right)^{-GAMP.CVT} - MU0P.CVT\right]}{1+\left(\frac{N}{CRN.CVT}\right)^{ALPHP.CVT}} - \frac{MU1N.CVT}{1+\left(\frac{CSP.CVT}{N}\right)^{BETAP.CVT}} \tag{3.7}$$

Table 3.1: Parameters for Equations 3.1 to 3.7

Statement	Parameter	Default	Units
MOBILITY	BN.CVT	4.75×10^{7}	cm/(a)
MOBILITY	BP.CVT	$9.925\times l0^{4}$	cm/ (a)
MOBILITY	CN.CVT	1.74×10^{5}	
MOBILITY	CP.CVT	8.842×10^{5}	
MOBILITY	TAUN.CVT	0.125	
MOBILITY	TAUP.CVT	0.0317	
MOBILITY	GAMN.CYT	2.5	
MOBILITY	GAMP.CVT	2.2	
MOBILITY	MUON.CVT	52.2	cm^{2}/ (v-a)
MOBILITY	MUOP.CVT	44.9	cm^{2}/ (v-a)
MOBILITY	MUIN.CVT	43.4	cm^{2}/ (v-a)
MOBILITY	MUIP.CVT	29.0	cm^{2}/ (v-a)
MOBILITY	MUMAXN.CVT	1417.0	cm^{2}/ (v-a)
MOBILITY	MUMAXP.CVT	470.5	cm^{2}/ (v-a)
MOBILITY	CRN.CVT	9.68×10^{14}	cm^{-3}
MOBILITY	CRP.CVT	2.23×10^{17}	cm^{-3}
MOBILITY	CSN.CVT	3.43×10^{20}	cm^{-3}
MOBILITY	CSP.CVT	6.10×10^{20}	cm^{-3}
MOBILITY	ALPHN.CVT	0.680	
MOBILITY	ALPHP.CVT	0.71	
MOBILITY	BETAN.CVT	2.00	
MOBILITY	BETAP.CVT	2.00	
MOBILITY	PCN.CVT	0.0	cm^{-3}
MOBILITY	PCP.CVT	0.23×10^{16}	cm^{-3}
MOBILITY	DELN.CVT	5.82×10^{14}	V/s
MOBILITY	DELP.CVT	2.054×10^{14}	V^{2}/s

The model for carrier emission and absorption processes proposed by Shockley-Read-Hall (SRH) was used to reflect the recombination phenomenon within the device. The electron and hole lifetimes τ_n and τ_p were modeled as concentration dependent. The equation is given by [23]:

$$R_{SRH} = \frac{pn - n_{ie}^2}{\tau_p\left[n + n_{ie}\exp\left(\frac{ETRAP}{kT_L}\right)\right] + \tau_n\left[p + n_{ie}\exp\left(\frac{-ETRAP}{kT_L}\right)\right]} \quad (3.8)$$

$$\tau_n = \frac{TAUN0}{1 + \frac{N}{(NSRHN)}} \quad (3.9)$$

$$\tau_p = \frac{TAUP0}{1 + \frac{N}{(NSRHP)}} \quad (3.10)$$

Here N is called the local (total) impurity concentration. The used parameters TAUNO, TAUPO, NSRHN and NSRHP are Table 3-2[23]. This model was activated with the CONSRH parameter of the MODELS statement.

Table 3.2: Default Parameters for Equations 3.8 to 3.10

Statement	Parameter	Default	Units
METERIAL	TAUNO	1.0×10^{-7}	s
METERIAL	NSRHN	5.0×10^{16}	cm^{-3}
METERIAL	TAUPO	1.0×10^{-7}	s
METERIAL	NSRHP	5.0×10^{16}	cm^{-3}

To account Bandgap narrowing effects, BGN model was used. These effects may be described by an analytic expression relating the variation in bandgap, ΔE_g, to the doping concentration, N. The expression used in ATLAS is from Slotboom and de Graaf [23]:

The used values for the parameters BGN.E, BGN.N and BGN.C are shown in Table 3.3[23].

Table 3.3: Default parameters of Slotbooms Bandgap Narrowing Model for equation 3.11

Statement	Parameter	Default	Units
MATERIAL	BGM.E	9.0×10^{16}	v
MATERIAL	BGN.N	1.0×10^{16}	cm^{-3}
MATERIAL	BGN.C	0.5	-

3.2 Simulation profile

Device simulation using silvaco atlas usually faces convergence problems and necessitates long run times.For this reason, the simulation of silicon nanowire MOSFET has been divided into a few groups. Firstly, Structure definition was performed. In this definition the simulation focused on creating the structure with a suitable mesh density. Regions and electrodes were defined as depicted in Fig. 3.2. Finer nodes were assigned in critical areas, such as across the gate oxide for an accurate 2 nm thickness to monitor channel activity and near the source/drain boundaries to get a better picture of the depletion layer and junction behavior. A coarser mesh was used elsewhere in order to reduce simulation run time.

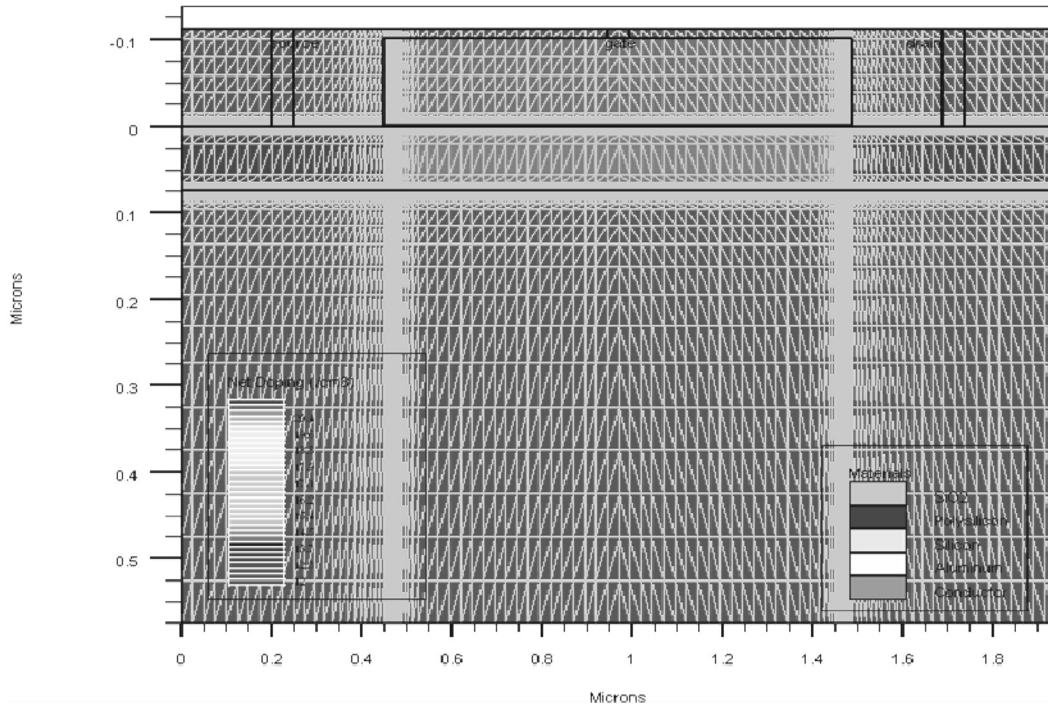

Figure 3.2: Cross-sectional view of p-type nanowire showing the mesh density used in this simulation.

Once the structure and the mesh were satisfactory, the simulation was performed with appropriate models as discussed in section 3.1 and numerical solving methods. The models were invoked by using the statements FERMI, CVT, CONSRH, BGN. The numerical solving methods GUMMEL, NEWTON were used to reduce the simulation run time, while keeping the accuracy of the simulation at a tolerable level.

To get convergence, a special bias point solving method was used. It was found that the simulation faced difficulty in solving at the initial desired bias points, i.e. 0.5 V, 1 V, 1.5 V and 2 V for drain voltage and 0V, - 0.5 V, -1 V,-1.5 V ,-2 V, -2.5 V and -3 V for gate voltage. Hence, the initial drain bias was set to 0.005 V and the next bias point was set to 0.05 V, before finally setting the bias point to desired value. For each biasing point a curve was generated for V g varying from 5 V to -5 V with decrement 0.025 V and Vd varying from 0 V to -10 V with decrement 0.05 V.

CHAPTER 4: RESULTS

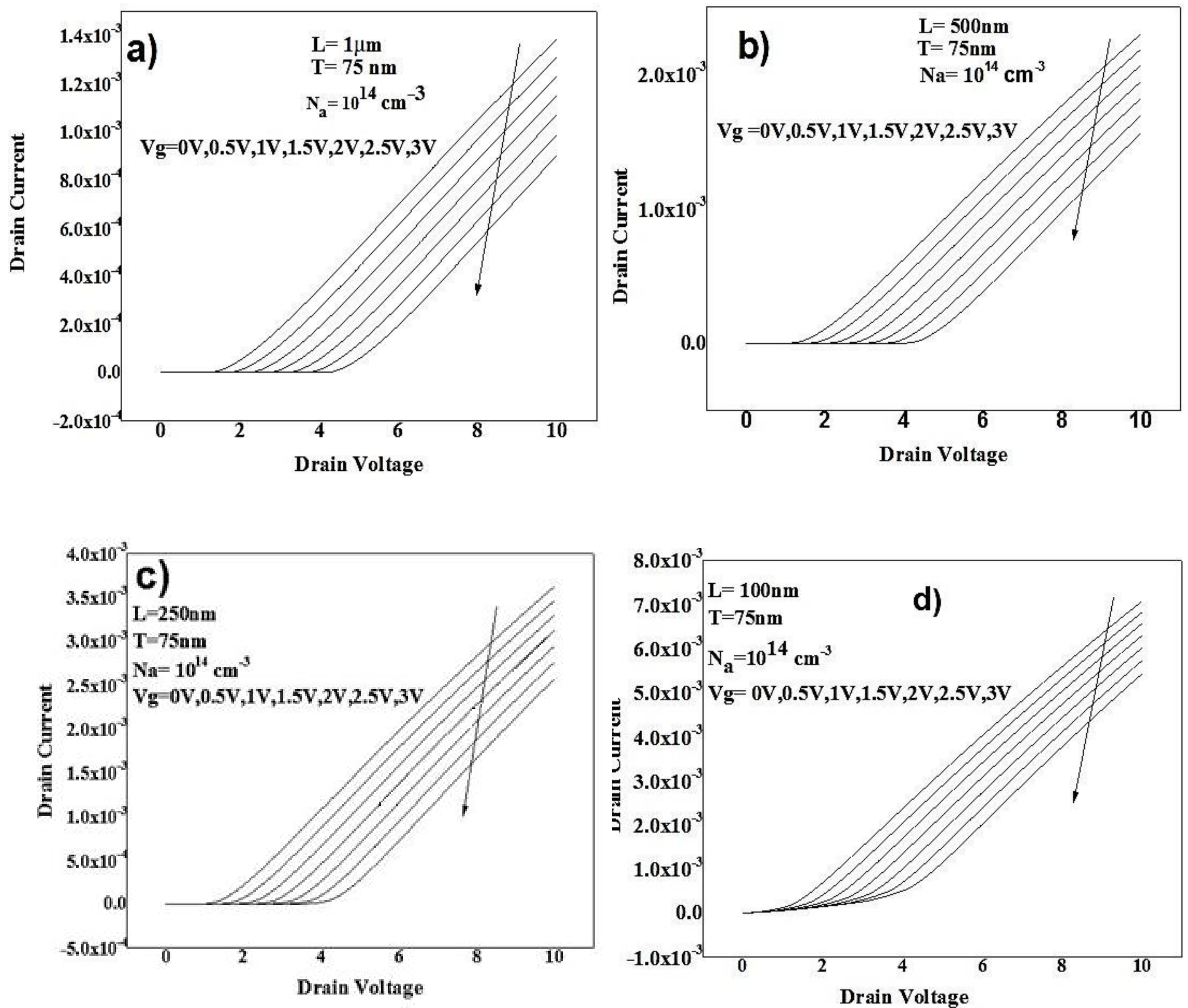

Fig. 4.1: Simulated output characteristics (I_D vs V_D) of Si-nanowires when both V_G and V_D are positive. The nanowires have thickness of 75nm, doping concentration of 10^{14} cm^{-3} and channel lengths of a) 1μm, b) 500nm, c) 250nm, d) 100nm. Different line represents I_D vs V_D curves for different gate voltages, i.e. 0V, 0.5V, 1V, 1.5V, 2V, 2.5V, 3V.

Fig. 4.1 shows the I_D-V_D characteristics of p-type Si-NWs for different channel lengths when both the gate voltage and drain voltages are positive. It is observed that, I_D-V_D curves are non-linear and there is no significant conduction up to a certain level of drain bias. The critical drain

voltage for one set of conduction (the drain voltage at which the conduction for $1e^{-4}$ A/µm level of current) is calculated for different channel lengths and for different values of gate voltages. When the channel length is 1µm (fig 4.1 a), the critical drain voltage is 2.43V for 0 gate voltage and 5.35V when gate voltage is 3V. When the channel length is 500nm (fig 4.1 b), the critical drain voltage is 1.98V for 0 gate voltage and 4.9V when gate voltage is 3V. When the channel length is 250nm (fig 4.1 c), the critical drain voltage is 1.65V for 0 gate voltage and 4.5V when gate voltage is 3V. When the channel length is 100nm (fig 4.1 d), the critical drain voltage is 0.925V for 0 gate voltage and 1.55V when gate voltage is 3V.

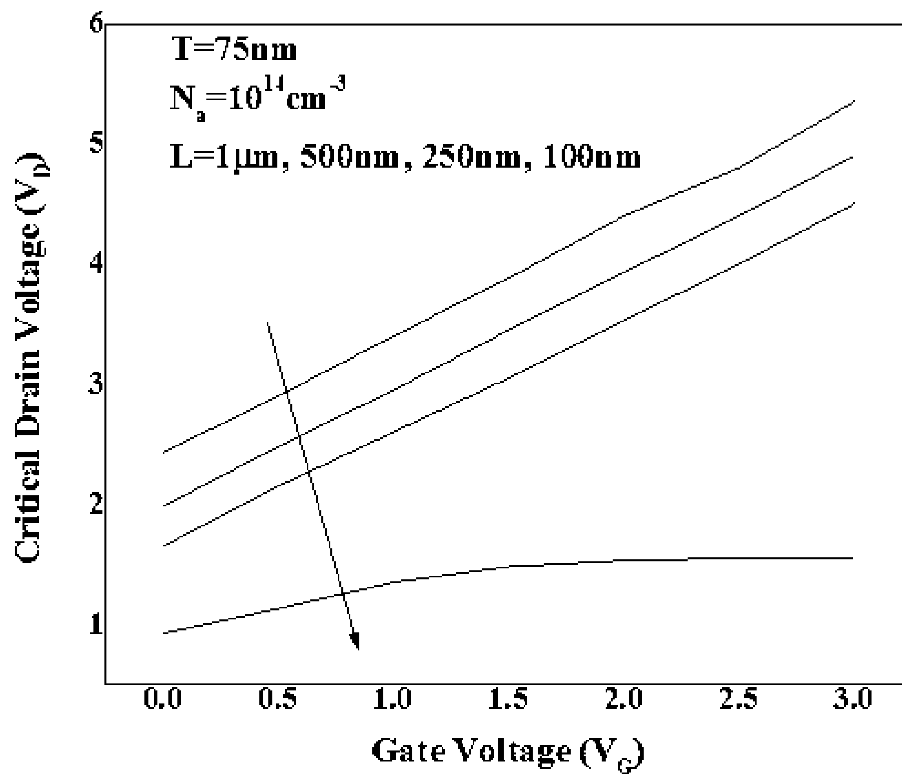

Fig. 4.2: Critical voltage vs gate voltage curve of Si-nanowire with nanowire thickness of 75nm and doping concentration of $10^{14}cm^{-3}$ for different channel lengths when both V_G and V_D are positive. Different lines represent curves for different channel lengths, 1µm, 500nm, 250nm and 100nm.

Fig 4.2 summarizes the critical V_D for conduction as a function of V_G for different channel lengths. It is observed that with the increase of V_G, critical drain voltage increases for any particular channel length and with the decreases of channel length, critical drain voltage decreases.

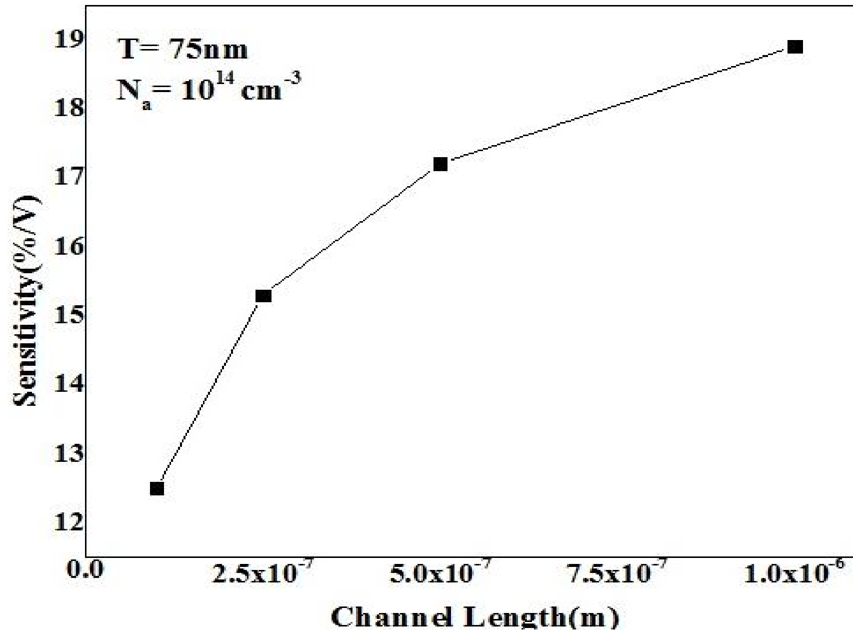

Fig. 4.3: Sensitivity vs channel length curve of Si-nanowire with nanowire thickness of 75nm and doping concentration of $10^{14}cm^{-3}$ for different channel lengths when both V_G and V_D are positive.

Fig 4.3 shows the sensitivity vs channel length when both V_G and V_D are positive. The sensitivity was calculated using first order calculation of $(I_1-I_2)/I_2/(V_{G1}-V_{G2})\times100$ for V_G change from 1.5 to 2V, at $V_D = 8V$ which is reasonable drain voltage for sufficient conduction of 75nm thick p-type Si NW at this mode of operation. It is found that the sensitivity of p-type Si NW is decreasing with the decrease of channel lengths with values for 1μm long Si NW of 18.9%/V and for 100 nm channel length of 12.5%/V.

Fig 4.4 shows the I_D-V_D characteristics of the NWs of 75nm thickness, when the gate voltage is positive and the drain voltage is negative for different channel lengths. All of the curves are nonlinear and none of them has reached to the saturation mode. From the figures it is clear that as the channel length decreases, the difference between the curves for different gate voltages are decreasing implying a significant reduction of gate effect at short channel lengths at this bias polarity condition. When the channel length is 100nm (fig 4.4 d) there is almost no difference between the curves. The critical drain voltage for one set of conduction (the drain voltage at which the conduction for $1e^{-12}$ A/μm level of current) is calculated for different channel lengths and for different values of gate voltages. When the channel length is 1μm (fig 4.4 a), the critical drain voltage is -9.83V for 0 gate voltage and -6.95V when gate voltage is 3V. When the channel length is 500nm (fig 4.4 b), the critical drain voltage is -5.43V for 0 gate voltage and -4V when gate voltage is 3V. When the channel length is 250nm (fig 4.4 c), the critical drain

voltage is -0.725V for 0 gate voltage and -0.85V when gate voltage is 3V. When the channel length is 100nm (fig 4.4 d), the critical drain voltage remains the same, - 0.00915V, for all the gate voltages.

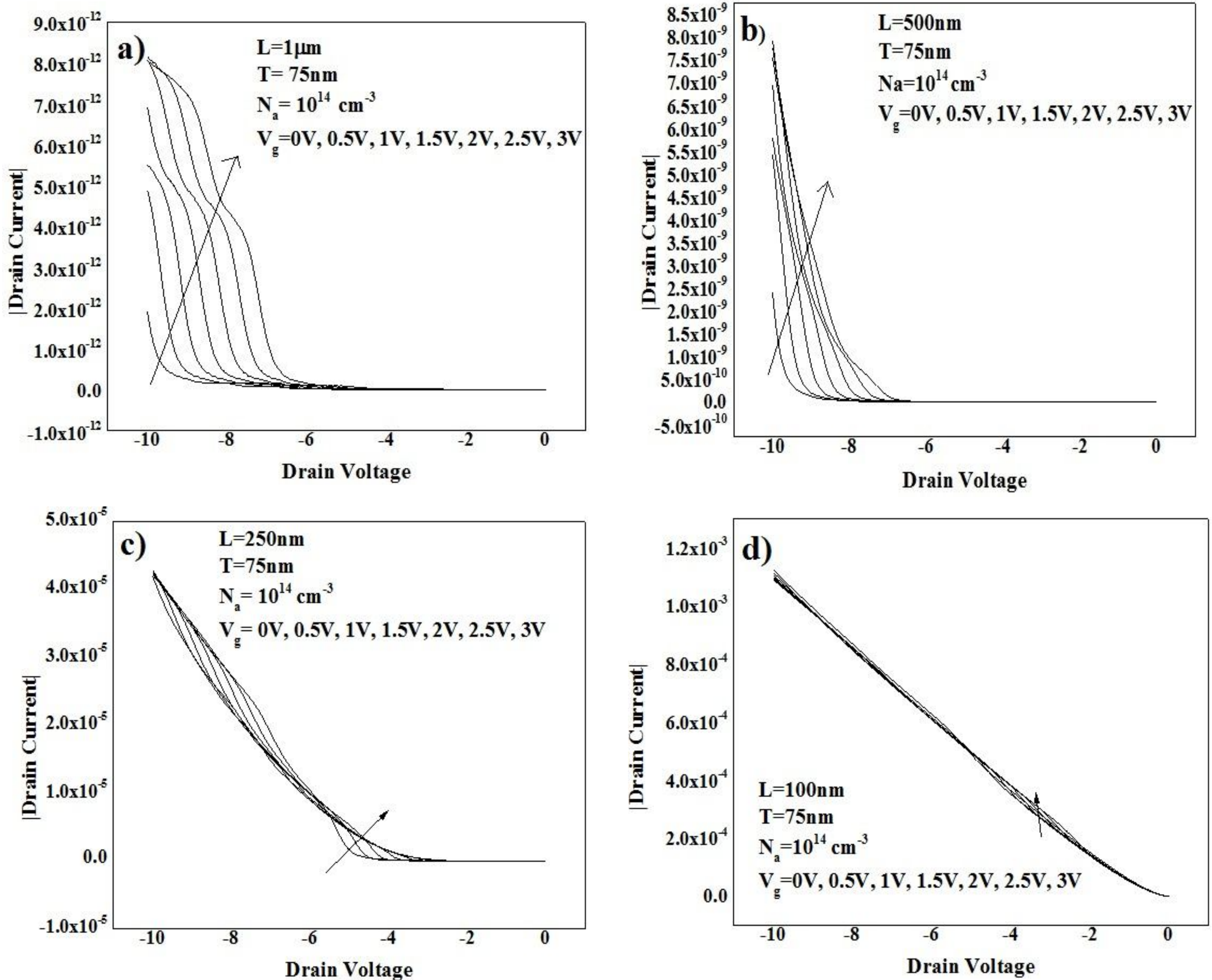

Fig. 4.4: Simulated output characteristics (I_D vs V_D) of Si-nanowires when V_G is positive and V_D is negative. The nanowires have thickness of 75nm, doping concentration of 10^{14} cm^{-3} and channel lengths of a) 1μm, b) 500nm, c) 250nm, d) 100nm. Different line represents (I_D vs V_D) curves for different gate voltages, i.e. 0V, 0.5V, 1V, 1.5V, 2V, 2.5V, 3V.

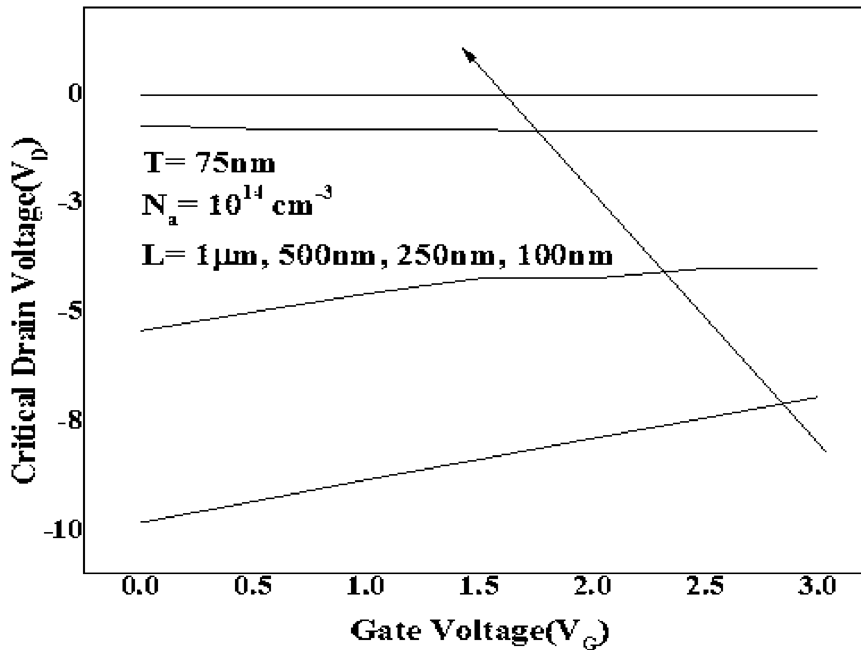

Fig. 4.5: Critical voltage vs gate voltage curve of Si-nanowire with nanowire thickness of 75nm and doping concentration of 10^{14} cm^{-3} for different channel lengths when V_G is positive and V_D is negative. Different lines represent curves for different channel lengths, 1μm, 500nm, 250nm and 100nm.

Fig 4.5 summarizes the critical V_D for conduction as a function of V_G for different channel lengths. It is observed that with the increase of V_G, critical drain voltage decreases for a certain channel length and with the decrease of channel length, critical drain voltage decreases. As the channel length decreases the effect of gate voltage on critical drain voltage also decreases. When the channel length becomes 100nm, there is no effect of gate voltage on the critical drain voltage.

Fig 4.6 shows the sensitivity vs channel length when V_G is positive and V_D is negative. The sensitivity was again calculated using first order calculation of $(I_1-I_2)/I_2/(V_{G1}-V_{G2})\times100$ for V_G change from 1.5 to 2V, at V_D = -9V which is reasonable drain voltage for sufficient conduction of 75nm thick p-type Si NW at this mode of operation. It is found that at this mode of operation, sensitivity again decreases rapidly with the decrease of channel length. The sensitivity for 1μm long Si NW is 124.4%/V which reduces to value of 5.7%/V for 100nm channel length. However, it is worth mentioning that the theoretical sensitivity above 120% for 1 μm and 500 nm Si NWs at this mode of operation are not practically achievable due to pico and nano ampere range of conduction which is very difficult for measurement using conventional parameter analyser. For 250 nm and 100 nm channel lengths although quite a reasonable conduction is exhibited the gate effect is diminished which implies that at this mode of conduction p-type Si NW might not be used as biosensors.

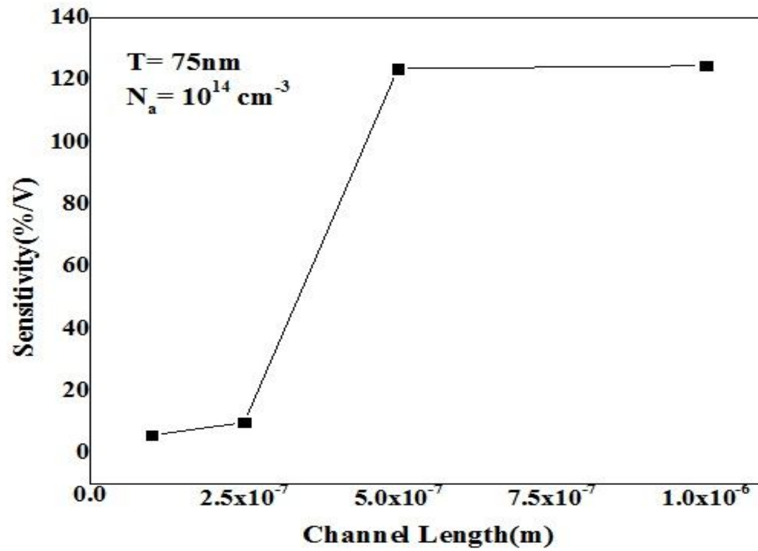

Fig. 4.6: Sensitivity vs channel length curve of Si-nanowire with nanowire thickness of 75nm and doping concentration of 10^{14}cm^{-3} for different channel lengths when V_G is positive and V_D is negative.

Fig. 4.7 shows the I_D-V_D characteristics, when the gate voltage is negative and the drain voltage is positive for SI-NWs with a NW thickness of 75nm and for different channel lengths. At this mode of operation significant conduction can be seen and the I_D-V_D characteristics are becoming reasonably linear with more negative gate voltages, but none of them has reached to the saturation mode for drain bias up to 10 V. This behavior is similar to the behavior observed by Chen et al [20]. The critical drain voltage for one set of conduction (the drain voltage at which the conduction for 1e^{-4} A/μm level of current) is again calculated for different channel lengths and for different values of gate voltages. When the channel length is 1μm (fig 4.7 a), the critical drain voltage is 2.43V for 0 gate voltage and 0.55V when gate voltage is 3V. When the channel length is 500nm (fig 4.7 b), the critical drain voltage is 1.98V for 0 gate voltage and 0.275V when gate voltage is 3V. When the channel length is 250nm (fig 4.7 c), the critical drain voltage is 1.65V for 0 gate voltage and 0.15V when gate voltage is 3V. When the channel length is 100nm (fig 4.7 d), the critical drain voltage is 0.925V for 0 gate voltage and 0.075V when gate voltage is 3V.

Fig 4.8 summarizes the critical V_D for conduction as a function of V_G for different channel lengths. It is observed that with the increase of negative V_G, critical drain voltage decreases for a particular channel length and with the decrease of channel length, critical drain voltage decreases.

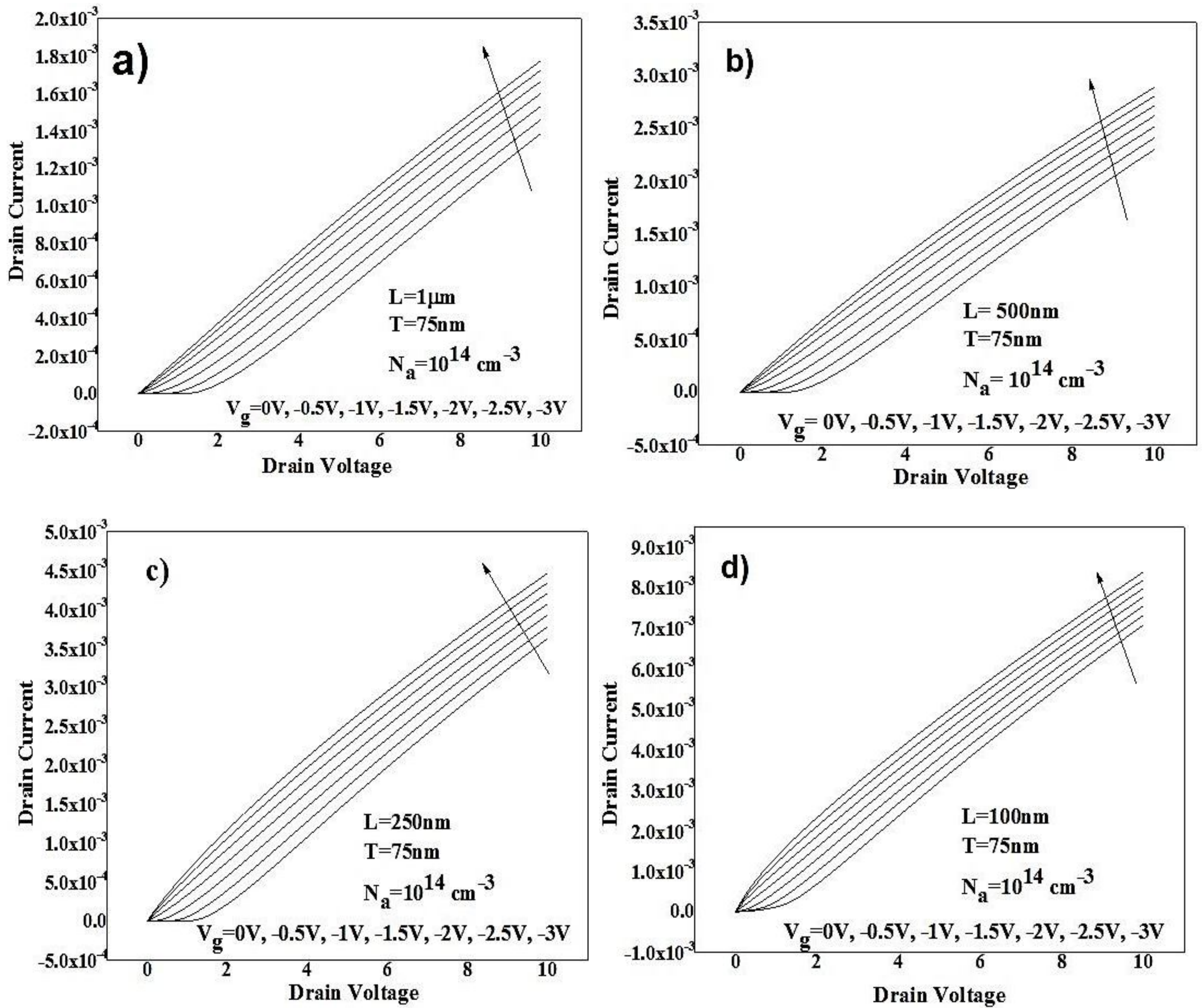

Fig. 4.7: : Simulated output characteristics (I_D vs V_D) of Si-nanowires when V_G is negative and V_D is positive. The nanowires have thickness of 75nm, doping concentration of 10^{14} cm^{-3} and channel lengths of a) 1µm, b) 500nm, c) 250nm, d) 100nm. Different line represents I_D vs V_D curves for different gate voltages, i.e. 0V, -0.5V, -1V, -1.5V, -2V, -2.5V, -3V.

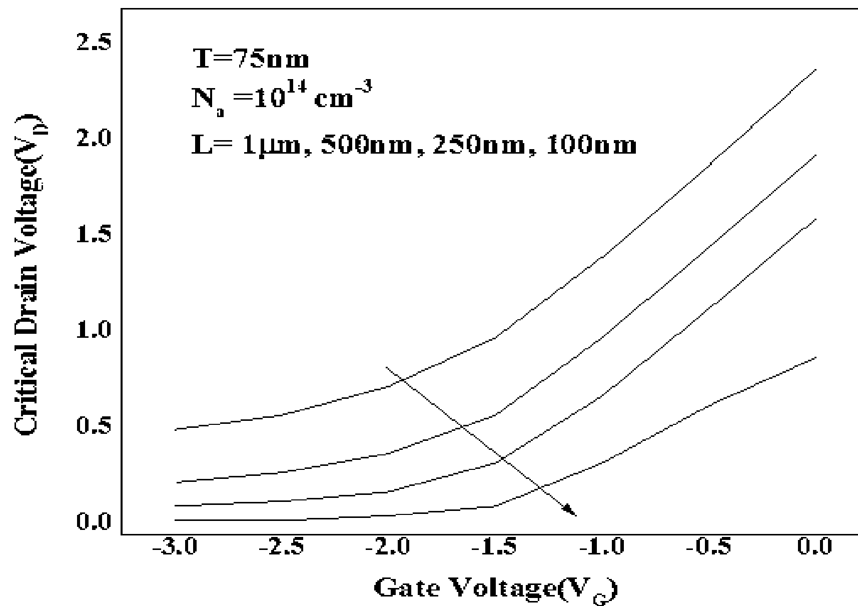

Fig. 4.8: Critical voltage vs gate voltage curve of Si-nanowire with nanowire thickness of 75nm and doping concentration of $10^{14}cm^{-3}$ for different channel lengths when V_D is positive and V_G is negative. Different lines represent curves for different channel lengths, 1µm, 500nm, 250nm and 100nm.

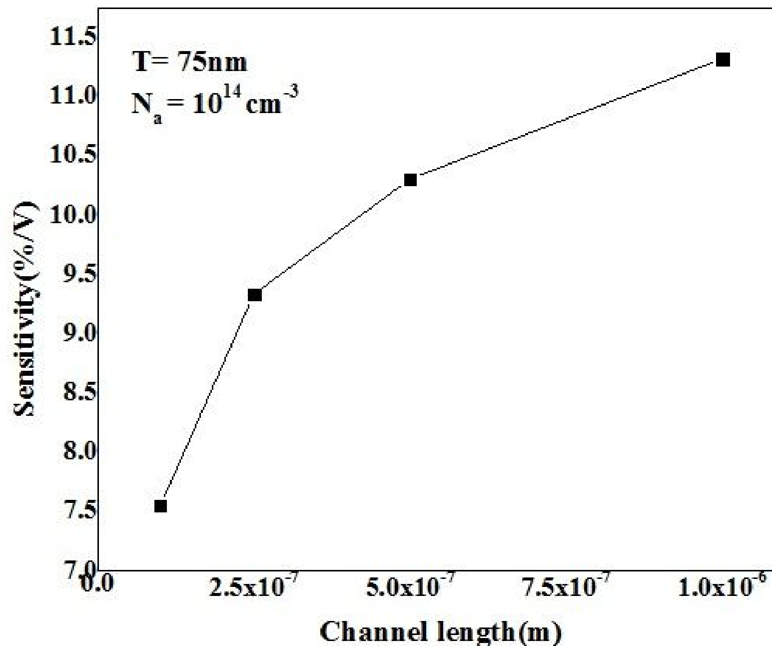

Fig. 4.9: Sensitivity vs channel length curve of Si-nanowire with nanowire thickness of 75nm and doping concentration of $10^{14}cm^{-3}$ for different channel lengths when V_G is negative and V_D is positive.

Fig 4.9 shows the sensitivity vs channel length when V_D is positive and V_G is negative. The sensitivity was again calculated using first order calculation of $(I_1-I_2)/I_2/(V_{G1}-V_{G2})\times100$ for V_G change from -1.5 to -2V, at V_D = 8V which is reasonable drain voltage for sufficient conduction of 75nm thick p-type Si NW at this mode of operation. It is found that the sensitivity for 1μm long Si NW is 11.318%/V which decreases to a value of 7.549%/V at 100nm channel length.

Fig. 4.10 shows the I_D-V_D characteristics of the NWs of 75nm thickness, when both the gate voltages and the drain voltages are negative for different channel lengths. A drastic change of the NW characteristics is observed and the the 75nm thick NWs are behaving perfectly as a transistor. For all these channel lengths reasonable saturation is exhibited at the drain voltage around -1.5V however for the channel length of 100nm (fig 4.10 d), the I_D-V_D characteristic's uprising is indicating the presence of short channel effects.

Fig 4.11 shows the sensitivity vs channel length when both V_G and V_D are negative. The sensitivity was again calculated using first order calculation of $(I_1-I_2)/I_2/(V_{G1}-V_{G2})\times100$ for different V_G changes, at V_D = -8V which is reasonable drain voltage for sufficient conduction of 75nm thick p-type Si NW at this mode of operation. It is observed that in this mode of operation sensitivity is very high compare to the other modes of operation for all channel lengths. For 1μm channel length, sensitivities obtained are 199.866%/V (when ΔV_G =1-1.5), 154.373%/V (when ΔV_G =1.5-2) and 103.604%/V (when ΔV_G =2.5-2). For 100nm channel length, sensitivities obtained are 35.019%/V (when ΔV_G =1-1.5), 42.058%/V (when ΔV_G =1.5-2) and 38.333%/V (when ΔV_G =2.5-2). This result indicates that for p-type Si NW application of negative voltages to both V_G and V_D are the most viable mode for biosensor operation. However, the sensitivity might change depending on the gate voltage range.

To further characterize the NW behaviour, fig 4.12 shows the transfer characteristics (I_D-V_G curve) of silicon NW with a thickness of 75nm and for different channel lengths when V_D is positive and V_G is swapped from +5 V to -5V. It is found that the nanowires exhibit quite a good transistor behaviour especially for the channel length of 1μm and 500nm (Fig. 4.12 (a) and (b)) with sub threshold slope of 64.6 mv/dec and 69.4 mv/dec. For 250nm channel length, sub threshold slope is 101 mv/dec (Fig. 4.12 (c)) which reasonably good enough for biosensing operation. For the channel length of 100nm, although nanowire shows prominent short channel effect at high drain biases it can be still used as a good biosensor with a V_D of 0.5V. Fig. 4.12 reveals some crucial information about nanowire biosensor operation. For positive values of V_G and V_D the nanowire is actually in the off region and hence less gate sensitivity is expected as can be seen from maximum 19% sensitivity of 1 μm long Si NWs in Fig. 4.3. When V_G is negative and V_D is positive NWs can be set to exhibit excellent sensitivity with an appropriate V_G range if it can be ensured that NWs fall within the subthreshold region of operation.

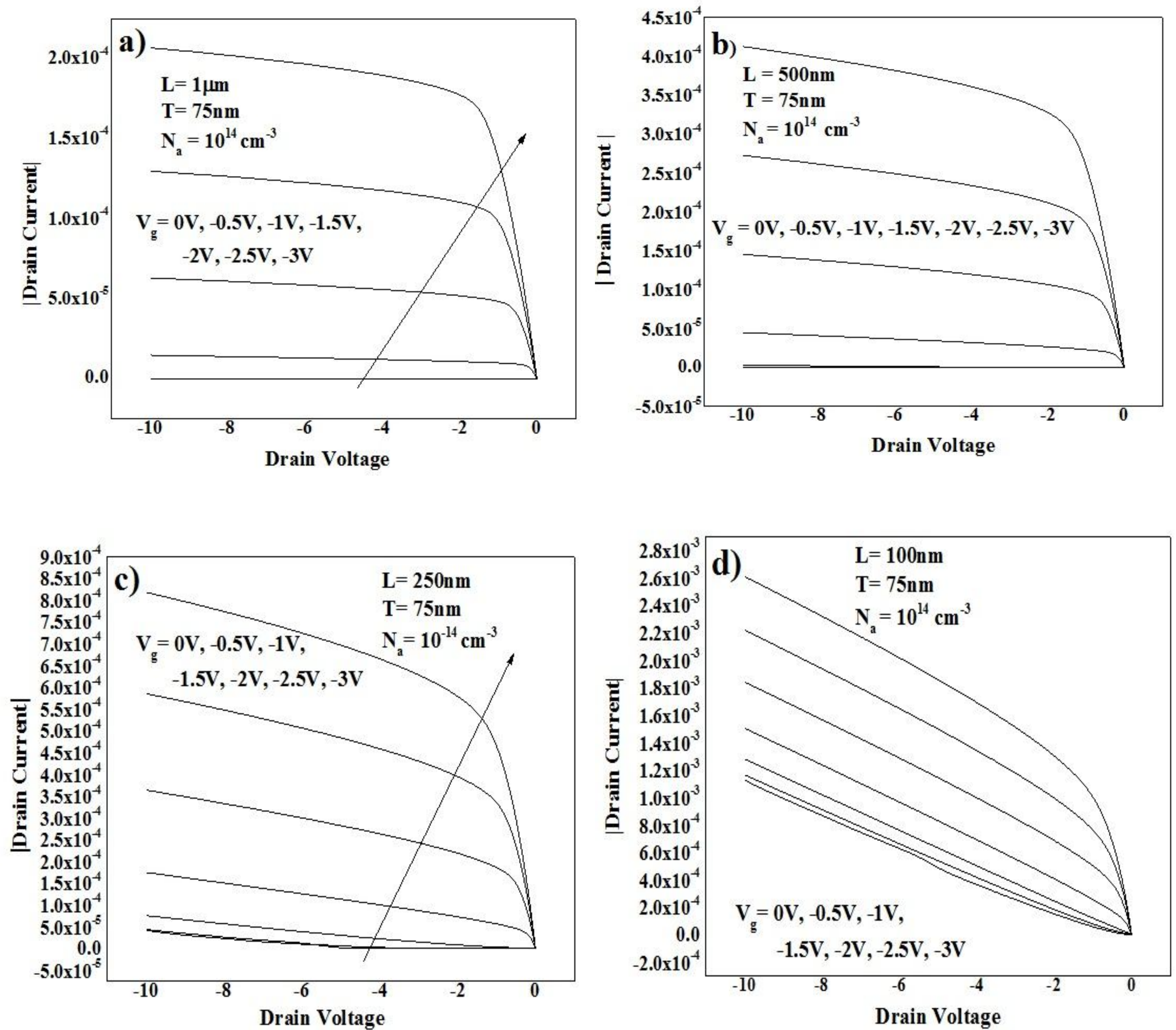

Fig. 4.10: Simulated output characteristics (I_D vs V_D) of Si-nanowires when both V_G and V_D are negative. The nanowires have thickness of 75nm, doping concentration of 10^{14} cm^{-3} and channel lengths of a) 1µm, b) 500nm, c) 250nm, d) 100nm. Different line represents I_D vs V_D curves for different gate voltages, i.e. 0V, -0.5V, -1V, -1.5V, -2V, -2.5V, -3V.

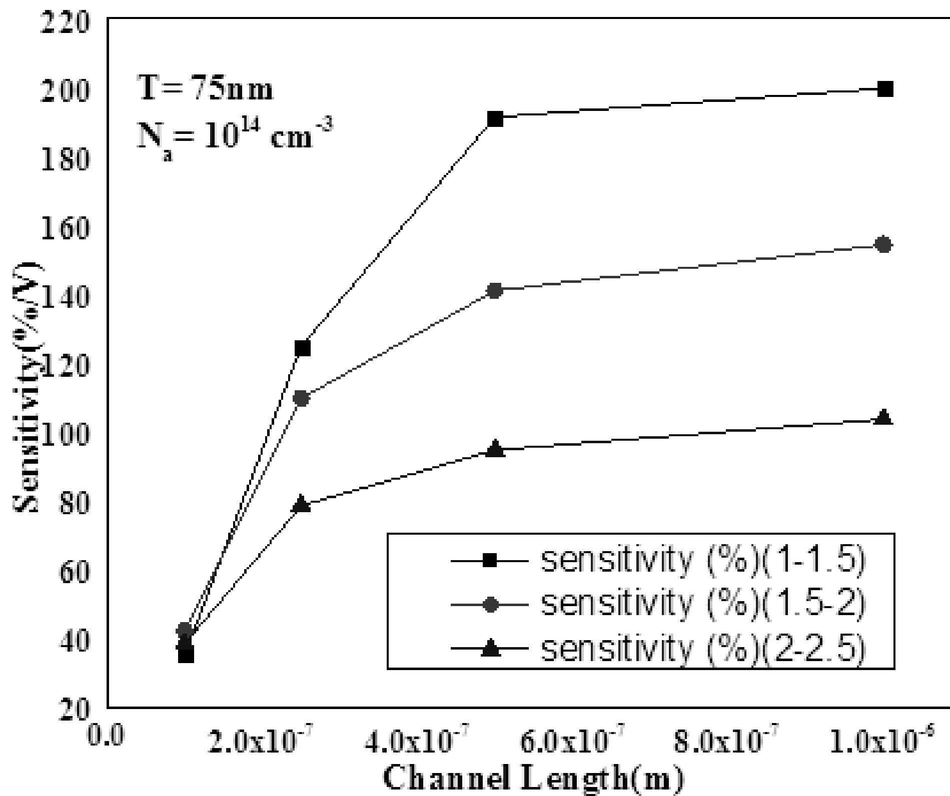

Fig. 4.11: Sensitivity vs channel length curve of Si-nanowire with nanowire thickness of 75nm and doping concentration of $10^{14}cm^{-3}$ for different channel lengths when both V_G and V_D are negative.

To explore this possibility, fig 4.13 shows the sensitivity vs channel length when V_D is positive with a set value of 0.5V and the gate voltage is swapped from -1V to -1.5 V ensuring subthreshold regime of operation. It can be seen that a very high sensitivity is achievable with values of 285.713%/V and 174.187%/V respectively for 1 μm and 100 nm channel lengths. These values are significantly higher that the sensitivity shown in Fig. 4.9 with similar operating condition, where V_G is negative and V_D is positive. However, in fig 4.9 the drain bias was set to 8 V and V_G was changed from -1.5 to -2V. Fig. 4.12 shows that at these values of V_G and V_D nanowires are actually in saturation regime thereby explaining lower sensitivity found in Fig. 4.9. This phenomenon also reveals the requirement of appropriate biasing for maximum sensitive operation of Si NW biosensors.

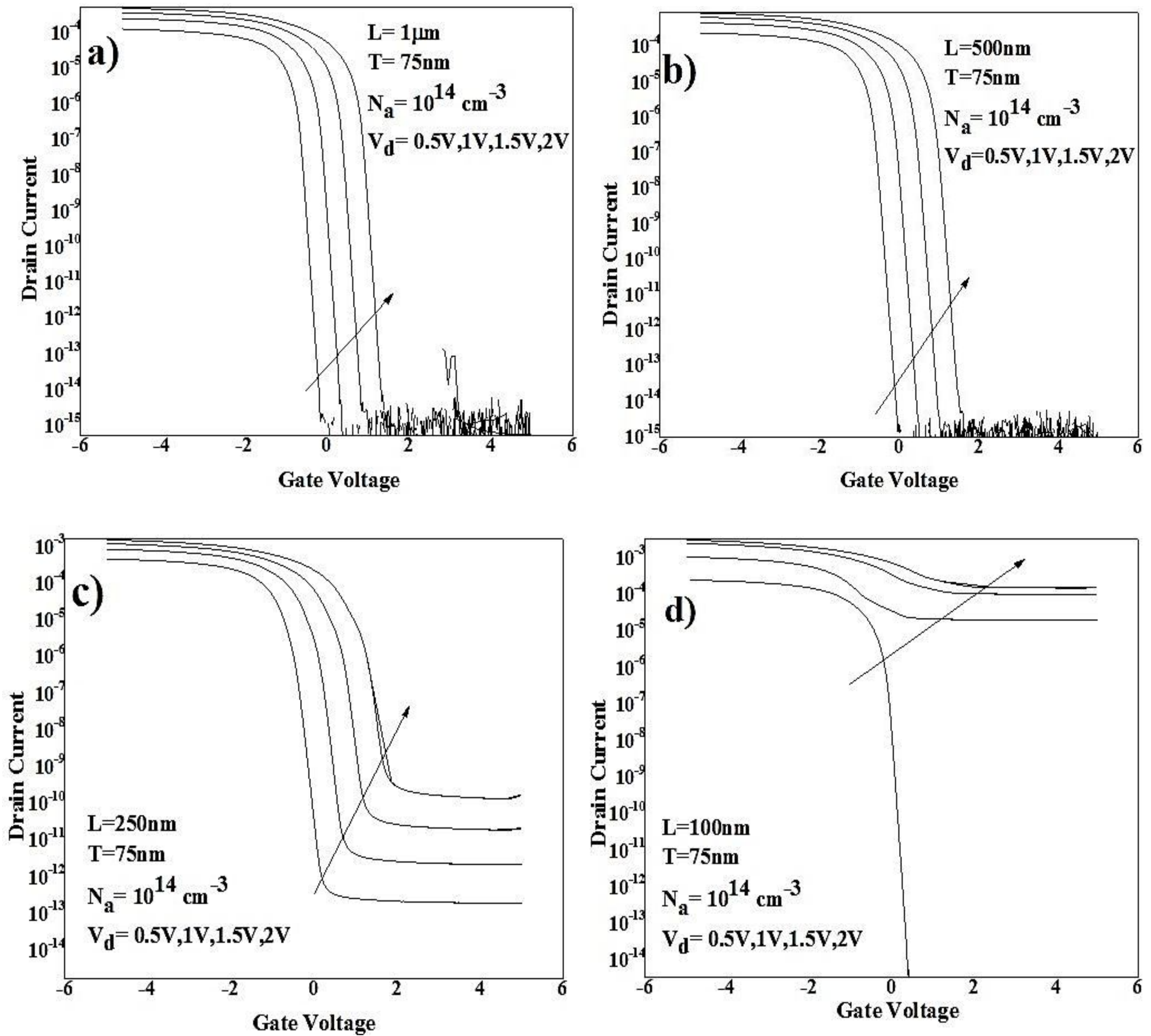

Fig. 4.12: Transfer characteristics (I_D vs V_G) of Si-nanowires when V_D is positive and V_G is swapped from +5V to -5V. The nanowires have thickness of 75nm, doping concentration of 10^{14} cm^{-3} and channel lengths of a) 1μm, b) 500nm, c) 250nm, d) 100nm. Different line represents I_D vs V_G curves for different drain voltages, i.e. 0.5V, 1V, 1.5V, 2V while V_G is swapped from 5 to -5.

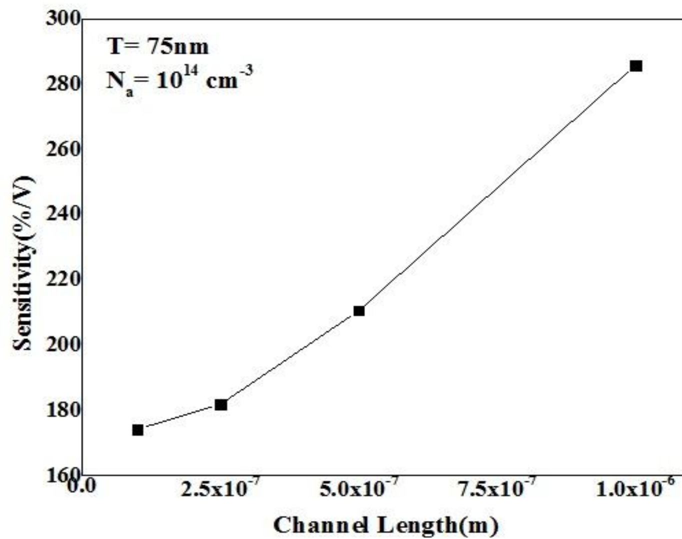

Fig. 4.13: Sensitivity vs channel lengths of Si-nanowires when V_D is positive with a set value of 0.5V and the gate voltage is swapped from -1V to -1.5 V ensuring subthreshold regime of operation.

Fig 4.14 shows the transfer characteristics (I_D-V_G curve) of silicon NW with a thickness of 75nm and for different channel lengths when V_D is negative and V_G is swapped from +5 V to -5V. These results are similar to the results of Fig. 4.12 except that DIBL has been significantly reduced in comparison to Fig. 4.12 for all channel lengths. Nanowires again exhibit quite a good transistor behavior for the channel length of 1μm, 500nm and 100 nm (Fig. 4.12 (a), (b) and (b)) with sub threshold slope of 63.2mv/dec, 69.4 mv/dec and 1900 mv/dec. For the channel length of 100nm, nanowire shows prominent short channel effect at all drain biases and hence, cannot be used as a good biosensor with a $V_D \geq 0.5$V. Fig. 4.14 also reveals some crucial information about nanowire biosensor operation. For positive values of V_G and negative values V_D the nanowire is actually in the off region and hence, cannot be used as a good biosensor. This conclusion agrees with the discussion of Fig. 4.6 with a similar mode of operation. However, when both V_G and V_D are negative NWs can again be set to exhibit excellent sensitivity with an appropriate V_G range if it can be ensured that NWs fall within the subthreshold region of operation.

To explore this possibility, fig 4.15 shows the sensitivity vs channel length when V_D is negative with a set value of -0.5V and the gate voltage is swapped from -1V to -1.5 V ensuring subthreshold regime of operation. It can be seen that quite a high value of sensitivity can be achieved for channel lengths of 1 μm, 500 nm and 250 nm with values of 307.6 %/V, 285.7 %/V and 249.9 %V respectively. For 100nm channel length, sensitivity is a bit reduced with the value of 77.264%/V due to the presence of short channel effects. However, these values are significantly higher than the values observed in fig. 4.11 with similar operating conditions which can be explained by the subthreshold regime of operation as discussed before.

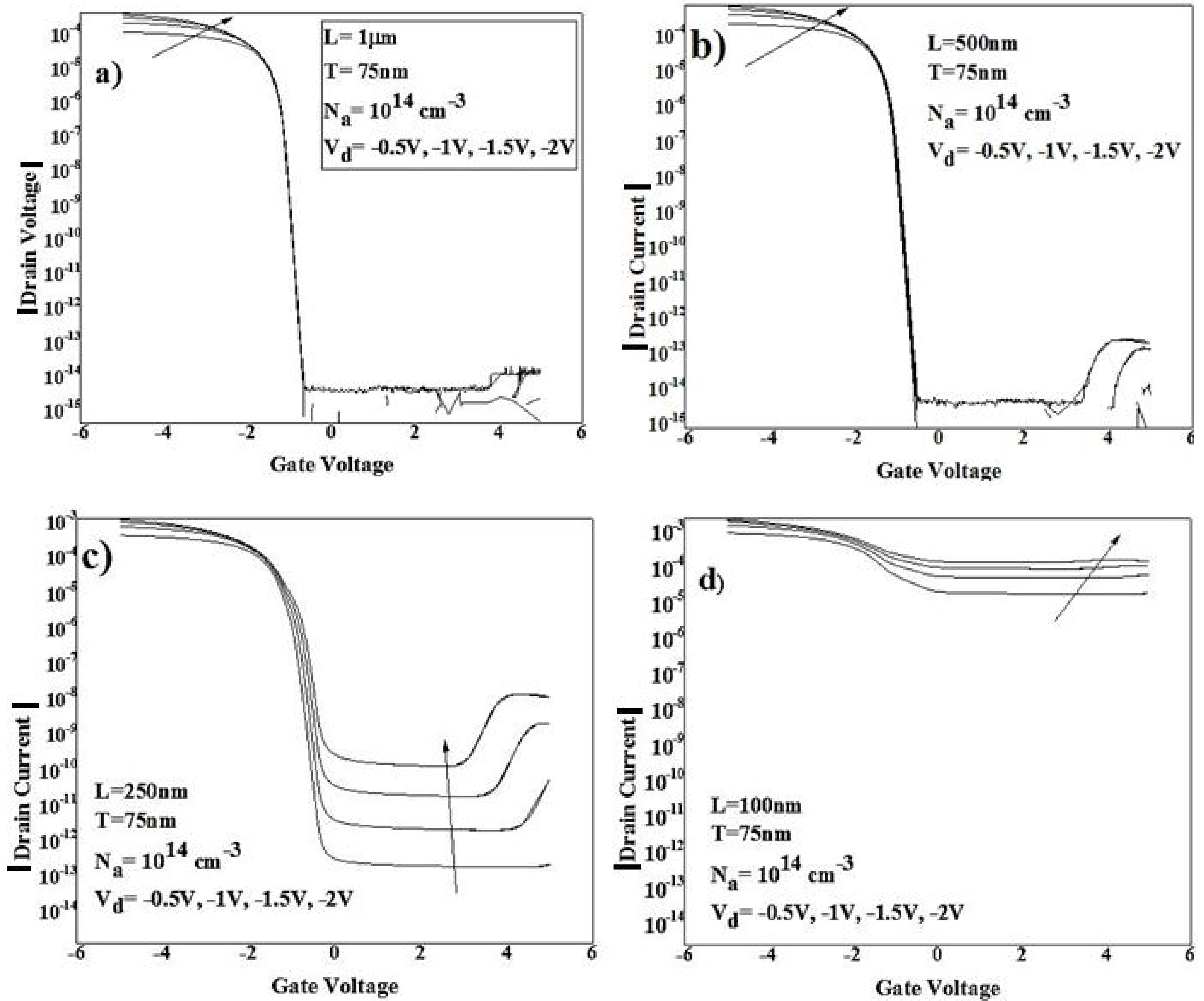

Fig. 4.14: Transfer characteristics (I_D vs V_G) of Si-nanowires when V_D is negative and V_G is swapped from +5V to -5V. The nanowires have thickness of 75nm, doping concentration of 10^{14} cm^{-3} and channel lengths of a) 1μm, b) 500nm, c) 250nm, d) 100nm. Different line represents I_D vs V_G curves for different drain voltages, i.e.- 0.5V, -1V, -1.5V,- 2V while V_G swapped from 5 to -5.

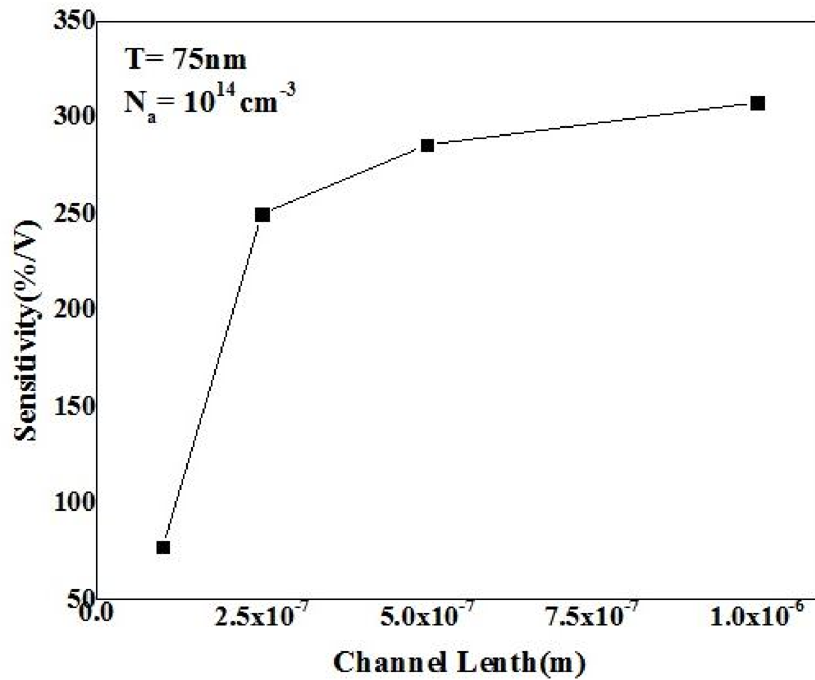

Fig. 4.15: Sensitivity vs channel length of Si-nanowires when V_D is negative with a set value of -0.5V and the gate voltage is swapped from -1V to -1.5 V ensuring subthreshold regime of operation.

CHAPTER 5: CONCLUSIONS, LIMITATIONS AND SCOPE OF FUTURE WORK

5.1 CONCLUSIONS:

We have investigated the effect of bias polarity on the DC electrical characteristics of p-type silicon nanowires and its effect on the gate sensitivity for possible application as biosensors. A 75 nm thick nanowire with doping concentration of 10^{14} cm^{-3} is investigated for different channel lengths. It is found that when drain and gate voltage both are positive nanowires I_D-V_D characteristics typically exhibit non-linear diode like characteristics with no appreciable conduction up to a certain level of drain bias. The critical drain bias for noticeable conduction is extracted for different channel lengths and for different values of gate voltages. It is found that the critical drain bias for sufficient conduction increases with an increase of the positive values of gate voltage and decreases with the decrease of channel lengths. The gate sensitivity of nanowires at this mode of conduction is estimated and found to be 18.9%/V for a channel length of 1 µm which reduces to a value of 12.5%/V for the channel length of 100 nm.

When gate voltage is positive and drain voltage is negative no appreciable conduction is observed and the gate effect is diminished at short channel lengths which implies that at this mode of conduction p-type Si NW might not be suitable for biosensors. When gate voltage is negative and drain voltage is positive nanowires exhibit less non-linearity and with the increase of negative gate voltages perfectly linear characteristics is achieved through the accumulation of holes in the nanowire by the gate effect. The critical drain bias for sufficient conduction is also found to be significantly smaller in comparison to results when both gate voltage is positive and when gate voltage is positive with negative drain voltages. The sensitivity of nanowires at this mode of operation is found to be 11.318%/V and 7.549%/V respectively for 1 µm and 100nm channel length for a gate voltage change from -2v to -1.5V with a drain bias set to 8V. This level of sensitivity agrees very well with the reported sensitivity of silicon nanowire biosensors.

However, when both gate and drain voltages are negative a drastic change of the nanowire characteristics is observed and the 75nm thick nanowires NWs are behaving perfectly as a transistor. It is observed that in this mode of operation sensitivity is very high compare to the other modes of operation for all channel lengths. For 1µm channel length, sensitivities obtained are 199.866%/V (when ΔV_G =1-1.5), 154.373%/V (when ΔV_G =1.5-2) and 103.604%/V (when ΔV_G =2.5-2). For 100nm channel length, sensitivities obtained are 35.019%/V (when ΔV_G =1-1.5), 42.058%/V (when ΔV_G =1.5-2) and 38.333%/V (when ΔV_G =2.5-2). This result indicates that for p-type Si NW application of negative voltages to both V_G and V_D are the most viable mode for biosensor operation.

We also investigated sub-threshold characteristics of nanowires and it is observed that nanowires can be set to exhibit excellent sensitivity with an appropriate V_G range if it can be ensured that NWs fall within the sub-threshold region of operation. Sensitivity values of 285.713%/V and 174.187%/V are achieved respectively for 1 µm and 100 nm channel lengths with positive drain voltage and negative gate voltages and sensitivity values of 307.6 %/V and 285.7 %/V are achieved

respectively for 1 μm and 100 nm channel lengths with negative voltages both at drain and gate ensuring subthreshold regime of operation. This investigation reveals the requirement of appropriate biasing scheme for highly sensitive biosensor operation and is very significant for nanowire based biosensor applications as transistor behavior can be set by choosing appropriate bias conditions which would allow large conductance charge upon attachment of Biomolecules and a highly sensitive biosensor could be realized.

5.2 LIMITATIONS AND SCOPE OF FUTURE WORK:

- This investigation is done using classical 2D simulation in ATLAS frame work. For nanowires 3D simulation is usually expected to reveal more realistic results which obviously shows the requirement of 3D simulation.

- The simulation is done using classical drift diffusion model. The work could be extended for very constricted dimension nanowires with quantum model as bottom up grown nanowires have very small dimensions and potentially interesting for many applications like sensors, advanced electronic/photonic devices, heterogeneous integration of electronics with biology and energy harvesting.

- The simulation does not include lattice heating effects which is somehow imperative for nanowire devices simulation as huge heat generation by phonon drag effect usually affects nanowires. A simulation with energy balance model would be more accurate.

References

[1] M. Curreli, R. Zhang, F. Ishikawa, H-K. Chang, R.Cote, C. Zhou, and M. Thompson, "Real-time, label-free detection of biological entities using nanowire-based FETs," Nanotecnology, IEEE Transactions on, vol. 7, no. 6, pp. 651-667, novo 2008.

[2] Fernando Patolsky and Charles M. Lieber, “Nanowire Nanosensors”, materialstoday, pp. 20-28, Apr. 2005.

[3] A. Agarwal, W. L. Wong, K.L. Yang, S. Balakumar, N. Balasubramanian, A. Kwong, D. L. Trigg, N. Singh, C. Fang, C. Tung, and K. Buddharaju, "Silicon nanowire arrays for ultrasensitive label-free detection of DNA," International Conference on Solid State Devices and Metarials,PP. 18-21, Sep 2007.

[4] J. Hahm and C.M. Lieber, " Direct ultrasensitive electrical detection of DNA and DNA sequence variation using nanowire nanosensors," Nano Letters, vol. 4, pp. 51-54, 2004.

[5] S.E., J. F. Klemic, D.A. Routenberg, P.N. Wyrembak, D.B. Turner-Evans, A. D. Hamilton, D. A. LaVan, T. M. Fahmy, and M. A. Reed, "Label-free immunodetection with CMOS- compatible semiconducting nanowires," Nature, vol. 445, pp. 519-522,2007.

[6] W. U. Wang, C. Chen, K. Lin, Y. Fang, and C.M. Lieber, "Label-free detection of small molecules-protein interactions by using nanowire nanosensors," PNAS, vol. 102, no. 9, pp-3208-3212, March 2005.

[7] A.Kim, C.S. Ah, H. Y. Yu, J.-H. Yang, 1.-B.Baek, C.-G.Ahn, C.W. Park, M. S. Jun, and S. Lee, "Ultrasensitive, label-free , and real-time immunodetection using silicon field effect transistors," Applied physics Letters, Vol. 91, no. 10, pp. 103901-103903,2007.

[8] Y. Bunimovich, Y. Shin, W. Yeo, M. Amori, G. Kwong, and J. Heath, "Quantitative real time measurements of DNA hybridization with alkylated nanoxidized silicon nanowires in electrolyte solution," J. Am. Chern. Soc., vol. 128, pp. 16323-16331, Dec. 2006.

[9] Y. Wu,P. Hsu, C. Hsu, and W. Liu, "Polysilicon wire for the detection of label-free DNA," Journal of The Electrochemical Society, vol. 159, no. 6, pp.Jl91-Jl95, 2010.

[10] J. H. Chua, R.E. Chee, A. Agarwal, S.M. Wong, and G. Zhang, "Label-free electrical detection of cardiac biomarker with complementary metal-oxide semiconductor compatible silicon nanowire sensor arrays", Analytical Chemistry, vol. 81, no. 15, pp.6266-6271, 2009.

[11] N.Elfstrom, A. Karlstrom, and J. Linnors, "Silicon nanoribbons for electrical detection of biomolicules," Nano Letters, vol. 8, pp. 945-949, 2008.

[12] A. Cattani-Scholz, D.Pedone, M. Dubey, S. Peppi, S. Nickel, P. Feulner, J. Schwartz, G. Abstrelter, and M. Tornow, "Organophosphonate-based pnafunctionalization of silicon nanowires for label-free DNA detection," ACS NANO, vol. 2, no. 8, pp. 1653-1660,2008 .

[13] C. Lin, C. Hung, C. Hsiao, H. Lin, F. Ko, and Y. Yang, "Poly-silicon nanowire field-effect transistor for ultrasensitive and label-free detection of pathogenic avian influenza DNA," Biosensors and Bioelectronics, vol. 24, pp. 3019-3024,2009.

[14] Y. Chen, X. Wang, M. K. Hong, S. Erramilli, P. Mohanty and C. Rosenberg," Nanoscale Field Effect Transistors for Biomolecular Signal Amplification", Appl. Phys., Lett. 91, pp. 243511, 2007.

[15] F. Patolsky, G. Zheng and C.M. Lieber, "Nanowire-Based Biosensors," Anal. Chern. 78, pp. 4260-4269, 2006.

[16] A. Agarwal, 1. Lao, K. Buddharaju, N. Singh, N. Balasubramanian, and D. Kwong, "Silicon nanowire array bio-sensor using top-down CMOS technology," Solid-State sensors, Actuatorsand Microsystems Conference, 2007. TRANSDUSERS 2007, International, pp.1051-1054, 10-14, June 2007.

[17] P.Hsu, J. Lin, W. Hung, and A.cullis, "Ultra-sensitive polysilicon wire glucose sensornusing a 3-aminopropyltriethoxysilane and polydimethylsiloxne-treated hydrophobic fumed silica particle mixure as the sensing membrane", Sensors and Actuators B: Chemical, pp.273-279,2009.

[18] Mohammad M. A.Hakim,M.Lombardini, K.Sun,F.Giustiniano, P.L.Roach, D.E. Davies, P.H.Howarth, M. R. R.de Planque, H. Morgan, P. Ashburn, "Thin film polycrystalline silicon nanowire biosensors", Nano Letters, vol.12, Issue 4, pp.1868-1872,2012.

[19] Cui, Y., and Lieber,C. M., "Nanowire and Nano sensor for highly sensitive and selective detection of biological and Chemical species",Science,vol.293,pp1289-1292

[20] Songyue Chen, Johan G. Bomer, Wilfred G. van der Wiel, Edwin T. Carlen, and Albert van den Berg, "Top –Down Fabrication of Sub-30nm Monocrystalline Silicon Nanowires Using Conventional Microfabrication",American Chamical society ACSNANO, vol.3,No.11, pp. 3487-3490, 2009.

[21] J. Colinge, C. Lee, A. Afzalian, A. Dehdashti, 1. Yan, R. Ferain, P. Razavi, B. O'Neil, A. Blake, M. White, A. Kelleher, B. McCarthy, and R. Murphy, "Nanowire transistors without junctions," Nature Nanotechnology, vol. 5, pp. 225-229,2010.

[22] Zhiyong Zhang, Kun Yao, Yang Liu, Chuanhong Jin, Xuelei Liang, Quing Chen, and Lian-Mao Peng, "Qantitative Analysis of Current-Voltage Characteristics of semiconducting Nanowires: Decoupling of Contact effects",Wiley Inter Science,pp. ,2007.

[23] Atlas user's Manual: Device Simulation Software, 2008.

[24] C. J. Su, T. I Tasi, Y. L.Liou, Z. M Lin, H. C.Lin, and T.S. Chao, " Gate–All-Around Junctionless Transistors With Heavily Doped Polysilicon Nanowire Channels", IEEE Electron Device Letters, vol.32, no. 4, pp. 521-523, Apr. 2011.

APPENDIX A:

Table A.1: Data table of Critical drain voltages at which conduction level of current is $1e^{-4}$, Drive currents for ID-VD_VG(pos)_VD(pos)

Channel Length	Conduction level Of current	Gate Voltage (V)	Critical drain Voltage (V)	Drive current (A/µm)	Sensitivity (%/V)
1µm	$1e^{-4}$	0	2.43	$7.16e^{-4}$	18.9
		0.5	2.9		
		1	3.4		
		1.5	3.88		
		2	4.4		
		2.5	4.8		
		3	5.35		
500nm		0	1.98	$1.25e^{-3}$	17.2
		0.5	2.48		
		1	2.95		
		1.5	3.45		
		2	3.93		
		2.5	4.04		
		3	4.90		

Channel Length	Conduction level Of current	Gate Voltage (V)	Critical drain Voltage (V)	Drive current (A/µm)	Sensitivity (%/V)
250nm	$1e^{-4}$	0	1.65	$2.08e^{-3}$	15.3
		0.5	2.15		
		1	2.60		
		1.5	3.05		
		2	3.53		
		2.5	.00		
		3	4.50		
100nm		0	0.925	$4.43e^{-3}$	12.5
		0.5	1.13		
		1	1.35		
		1.5	1.48		
		2	1.53		
		2.5	1.55		
		3	1.55		

Table A .2: Data table of Critical drain voltages at which conduction level of current is 1e^{-12}, Drive currents for ID-VD_VG(pos)_VD(neg)

Channel Length	Conduction level Of current	Gate Voltage (V)	Critical drain Voltage (V)	Drive current (A/μm)	Sensitivity (%/V)
1μm	1e^{-12}	0	-9.83	-1.464e^{-12}	124.4445
		0.5	-9.35		
		1	-8.85		
		1.5	-8.38		
		2	-7.90		
		2.5	-7.43		
		3	-6.95		
500nm		0	-5.43	-3.18e^{-10}	123.4717
		0.5	-5.00		
		1	-4.58		
		1.5	-4.23		
		2	-4.03		
		2.5	-4.00		
		3	-4.00		

Channel Length	Conduction level Of current	Gate Voltage (V)	Critical drain Voltage (V)	Drive current (A/µm)	Sensitivity (%/V)
250nm	$1e^{-12}$	0	-0.725	$-2.54e^{-5}$	9.81219
		0.5	-0.800		
		1	-0.825		
		1.5	-0.825		
		2	-0.850		
		2.5	-0.850		
		3	-0.850		
100nm		0	-0.00915	$-8.56e^{-4}$	5.72178
		0.5	-0.00915		
		1	-0.00915		
		1.5	-0.00915		
		2	-0.00915		
		2.5	-0.00915		
		3	0.00457		

Table A.3: Data table of Critical drain voltages at which conduction level of current is $1e^{-4}$, Drive currents for ID-VD_VG(neg)_VD(pos)

Channel Length	Conduction level Of current	Gate Voltage (V)	Critical drain Voltage (V)	Drive current (A/µm)	Sensitivity (%/V)
1µm	$1e^{-4}$	0	2.43	$1.34e^{-3}$	11.31842
		0.5	1.93		
		1	1.45		
		1.5	1.03		
		2	0.775		
		2.5	0.625		
		3	0.550		
500nm		0	1.98	$2.30e^{-3}$	10.30459
		0.5	1.50		
		1	1.03		
		1.5	0.625		
		2	0.425		
		2.5	0.325		
		3	0.275		

Channel Length	Conduction level Of current	Gate Voltage (V)	Critical drain Voltage (V)	Drive current (A/µm)	Sensitivity (%/V)
250nm	$1e^{-4}$	0	1.65	$3.59e^{-3}$	9.33472
		0.5	1.18		
		1	0.725		
		1.5	0.375		
		2	0.225		
		2.5	0.175		
		3	0.150		
100nm		0	0.925	$6.79e^{-3}$	7.45949
		0.5	0.675		
		1	0.375		
		1.5	0.150		
		2	0.100		
		2.5	0.075		
		3	0.075		

Table A.4: Data table of Drive currents for ID-VD_VG(neg)_VD(neg)

<table>
<tr><th>Channel Length</th><th>Gate Voltage (V)</th><th>Drive current (A/µm)</th><th>Saturation Voltage (V)</th><th>Sensitivity (%/V)</th></tr>
<tr><td rowspan="7">1µm</td><td>0</td><td rowspan="7">$6.09e^{-5}$</td><td rowspan="7">-1.5</td><td rowspan="2">199.866</td></tr>
<tr><td>0.5</td></tr>
<tr><td>1</td><td rowspan="2">154.3728</td></tr>
<tr><td>1.5</td></tr>
<tr><td>2</td><td rowspan="3">103.604</td></tr>
<tr><td>2.5</td></tr>
<tr><td>3</td></tr>
<tr><td rowspan="7">500nm</td><td>0</td><td rowspan="7">$-1.37e^{-4}$</td><td rowspan="7">-1.5</td><td rowspan="2">191.4802</td></tr>
<tr><td>0.5</td></tr>
<tr><td>1</td><td rowspan="2">141.0285</td></tr>
<tr><td>1.5</td></tr>
<tr><td>2</td><td rowspan="3">94.6694</td></tr>
<tr><td>2.5</td></tr>
<tr><td>3</td></tr>
</table>

<table>
<tr><th>Channel Length</th><th>Gate Voltage (V)</th><th>Drive current (A/µm)</th><th>Saturation Voltage (V)</th><th>Sensitivity (%/V)</th></tr>
<tr><td rowspan="7">250nm</td><td>0</td><td rowspan="7">$-3.32e^{-4}$</td><td rowspan="7">Around -1.5V</td><td rowspan="2">124.7531</td></tr>
<tr><td>0.5</td></tr>
<tr><td>1</td><td rowspan="2">109.7132</td></tr>
<tr><td>1.5</td></tr>
<tr><td>2</td><td rowspan="3">78.4717</td></tr>
<tr><td>2.5</td></tr>
<tr><td>3</td></tr>
<tr><td rowspan="7">100nm</td><td>0</td><td rowspan="7">$-1.57e^{-3}$</td><td rowspan="7">Around -1.5V</td><td rowspan="2">35.01943</td></tr>
<tr><td>0.5</td></tr>
<tr><td>1</td><td rowspan="2">42.05802</td></tr>
<tr><td>1.5</td></tr>
<tr><td>2</td><td rowspan="3">38.3334</td></tr>
<tr><td>2.5</td></tr>
<tr><td>3</td></tr>
</table>

Table A.5 : Data table of Sub threshold slope(mv/dec), DIBL of different drain voltage for ID-VG_VD(pos)_VG -5 to 5

Channel Length	Sub threshold Slope for VD=0.5V (mv/dec)	DIBL	Sensitivity (%/V)
1µm	64.6	981.24	285.7132
500nm	69.4	891.9	210.52628
250nm	101	1192.2	181.8163
100nm	264	Not measureable	174.1871

Table A .6: Data table of Sub threshold slope(mv/dec), DIBL of different drain voltage for ID-VG_VD(neg)_VG -5 to 5

Channel Length	Sub threshold Slope for VD=0.5V (mv/dec)	DIBL	Sensitivity (%/V)
1µm	63.2	0	307.6893
500nm	69.4	0	285.712
250nm	100	500	249.9724
100nm	1190	950	77.2644